Ângela Rodrigues
Jesus Fernandes

Agregado de antenas 2x2 com polarização circular dual para constelações de satélites LEO

Dual circularly polarized 2x2 antenna array for LEO satellite constellations

Universidade de Aveiro
2021

Ângela Rodrigues Jesus Fernandes

Agregado de antenas 2x2 com polarização circular dual para constelações de satélites LEO

Dual circularly polarized 2x2 antenna array for LEO satellite constellations

Dissertação apresentada à Universidade de Aveiro para cumprimento dos requisitos necessários à obtenção do grau de Mestre em Engenharia Eletrónica e Telecomunicações, realizada sob a orientação científica do Doutor João Nuno Matos, Professor associado do Departamento de Eletrónica, Telecomunicações e Informática da Universidade de Aveiro, e do Doutor Tiago Varum, investigador no Instituto de Telecomunicações.

o júri / the jury

Presidente / President

Prof. Doutor Armando Carlos Domingues da Rocha
professor auxiliar da Universidade de Aveiro

Vogais / Examiners comittee

Prof. Doutor Henrique Manuel de Castro Faria Salgado
professor associado da Faculdade de Engenharia da Universidade do Porto (arguente)

Prof. Doutor João Nuno Pimentel da Silva Matos
professor associado da Universidade de Aveiro (orientador)

agradecimentos

Antes de mais quero agradecer aos meus pais por me terem dado a oportunidade de chegar até aqui.

Ao meu namorado e às minhas amigas pelo apoio incondicional e por não me deixarem nunca desistir. À Tânia por me vir sempre buscar às 17h para a pausa do lanche.

Aos meus orientadores, o professor Nuno Matos e o Doutor Tiago Varum, pelo acompanhamento e compreensão que me proporcionaram. Um agradecimento especial à Amélia pela paciência e disponibilidade para me ajudar.

Ao Instituto de Telecomunicações pela disponibilização do espaço e recursos que permitiram a conclusão desta dissertação e ao Hugo Mostardinha pelo apoio técnico.

palavras-chave

Antenas microstrip, alimentação por fenda, agregado de antenas, polarização circular

resumo

Apesar das tecnologias de comunicações estarem em rápido desenvolvimento, ainda há muitas regiões remotas que não são abrangidas por serviços de telecomunicações. Constelações de satélites LEO estão a ser usados para abordar este problema, com o objetivo de providenciar serviços de comunicação globais contínuos e de alta capacidade. As comunicações satélite são usualmente feitas perto da banda Ka, com frequências mais altas para o uplink e mais baixas para o downlink. A antena desenvolvida nesta dissertação foi projetada para operar a 20GHz, podendo ser implementada para as comunicações downlink. Adicionalmente, antenas com polarização circular são úteis em comunicações satélites pela versatilidade de serem capazes de receber outras polarizações.

A antena proposta é uma patch quadrada com alimentação por acoplamento através de fenda, em dois pontos ortogonais, integrada com um acoplador híbrido em quadratura e mais tarde incluída num array 2x2. Esta antena tem a possibilidade de ter polarização circular esquerda ou direita consoante a escolha do porto de alimentação.

As estruturas apresentadas foram modeladas progressivamente por simulação, em várias fases, e por isso a evolução dos resultados puderam ser analisados à medida que a antena ficava mais complexa. Depois a antena projetada foi fabricada e foram efetuadas medições para validação.

keywords Microstrip antennas, aperture coupled feed, antenna array, circular polarization

abstract

Although communications technologies are in rapid development, there are still many remote regions that aren't covered by telecommunication services. LEO satellite constellations are being used to address this issue by aiming to provide continuous and high-capacity global communication services. Satellite communications are usually made using frequencies near the Ka band, with higher frequencies for the uplink and lower frequencies for the downlink. The antenna developed in the course of this dissertation was chosen to operate at 20GHz, enabling its implementation for downlink communications. Furthermore, circular polarized antennas are useful in satellite communications for versatility by being able to receive other polarizations.

The proposed antenna is a dual-fed square patch, with aperture coupled feed, incorporated with a quadrature hybrid coupler as the feed and later included in a 2x2 array. This antenna has the possibility of being left or right circularly polarized by choosing the feeding port.

The structures presented were modeled progressively by simulation, in several stages, and so the evolution of the results could be analyzed as the antenna got more complex. After designing the antenna it was later fabricated, and measurements were taken for validation.

Contents

List of Figures

List of Tables

1 Introduction

1.1 Background

"Telecommunication is a technology that eliminates distance between continents, between countries, between persons."[1]

Technological evolution has been greatly accentuated in recent years, giving rise to new technologies and services, especially in the field of wireless communications. For centuries mankind has tried to find and develop new ways to communicate with one another at a distance in more efficient and practical ways. Starting with the use of messengers and smoke signals, to the telegraph, to the telephone and radio transmission, this long-distance communication has been made easier and more accessible to all.

The genesis of modern telecommunications occurred in the nineteenth century, with the discovery of electromagnetism. In 1820, the electromagnetic field due to electric current was discovered by Hans Oersted [2]. By 1864, James Maxwell had compiled the well-known Maxwell equations, mathematical formulas for the propagation of electromagnetic waves (at this point still not proven [1]). Between 1886 and 1889, Heinrich Hertz provided the basis for radio transmission by proving the existence of electromagnetic radiation. This work was followed up by Marconi who was successful in radio transmission of a signal, thus inventing the radio [3].

After the invention of the radio, countless advances have been made in this field to achieve the systems we have today. Nowadays, telecommunications have become an essential part of society, the economy, and science. However, the requirements for wireless systems also became stricter as the technology advanced and the need to improve them has motivated even more investigations in this field.

Antennas are a fundamental (and one of the most critical) element of radio systems since they allow the transition between a guided wave and a 'free-space' wave, and vice-versa [4]. They greatly influence the radiated waves and therefore must be designed to fulfill the requirements of the system presents. There are various types of antennas, with different shapes, configurations, complexity, and characteristics. Simple radiating elements can also be grouped in arrays to improve parameters such as gain and directivity when the radiation requirements can't be achieved with individual elements.

In this dissertation, the focus will be on microstrip antennas, which became popular in the 1970s for airborne applications, such as airplanes, missiles and spacecrafts [4]. Nowadays they continue being widely used for government and commercial applications due to their versatility and low cost [5]. Since their invention, the demand has increased rapidly and thus the necessity to enhance their performance has also risen. In order to reduce their overall size and performance characteristics, different configurations have been developed such as non-contacting excitation methods [6]–[8], multilayer designs [9], irregular patch shapes [10], [11], different materials [10], [12] and aggregation in arrays [13]. It is expectable that the demand for microstrip antennas will continue to grow, being incorporated in more and more applications.

Even though communications technologies are in rapid development, there are still many remote regions, for example, that aren't reached by telecommunication services [14]. To assure the distribution of services to these locations, many projects have started targeting LEO (Low Earth Orbit) satellite constellations development to address this problem. The goal is to achieve continuous and high-capacity global communication services [15]. Usually, satellite communications occupy frequencies near the Ka band, with higher frequencies for the uplink and lower frequencies for the downlink. This is because emitting at a higher frequency requires more power, so it is logic that the satellite emits at a lower frequency due to low power requirements which aren't as strict in ground stations. The antenna proposed in this dissertation was chosen to operate at 20GHz, allowing its implementation for downlink communications. On the other hand, the use of a circularly polarized antenna also has advantages because it provides versatility (it is compatible with other polarizations) [16].

1.2 Objectives

The purpose of this dissertation is the development of a circularly polarized aperture coupled microstrip square patch antenna, using a quadrature hybrid coupler for the feed. This allows the selection of which circular polarization is obtained at a given time – LHCP (Left Hand Circular Polarization) or RHCP (Right Hand Circular Polarization) - as well as improved bandwidth.

This antenna will then be incorporated into a 2x2 array, with half-wavelength spacing and 90º progressively rotated elements. The array should have enhanced gain and wider circular polarization bandwidth compared to the individual element.

The use of the electromagnetic simulation software CST Studio Suite will facilitate a more accurate design of the structures proposed, enabling the monitoring of the antenna's estimated measurements as it is developed.

1.3 Outline

This document is divided into five main chapters. The first, and current, chapter is a brief introduction to the motivation and objectives of this dissertation. Chapter number two contains relevant theoretical background, essential to the understanding of the work done. An explanation of antennas' main principles of functioning is given, several types of antennas are presented and described, and the main antenna parameters explained. In chapter 3, the microstrip antennas are singled out and their method of design is described. Simulations are also presented as a method for antenna design and modelling. In chapter 4 the implementation of the antennas design in the previous chapter is introduced and the corresponding results displayed and discussed. Finally, chapter 5 sums up the dissertation's conclusions and what future work may still be in order.

2 Antenna theory

An antenna is essentially “a means for radiating or receiving radio waves” [17]. This device is therefore an indispensable part of any wireless system since it makes the bridge between the guided and free-space transmission, as is depicted in Figure 1. The existence of variable currents in the antenna causes electromagnetic waves to radiate from it into the free-space. Thus, a good antenna design is vital for an appropriate system performance.

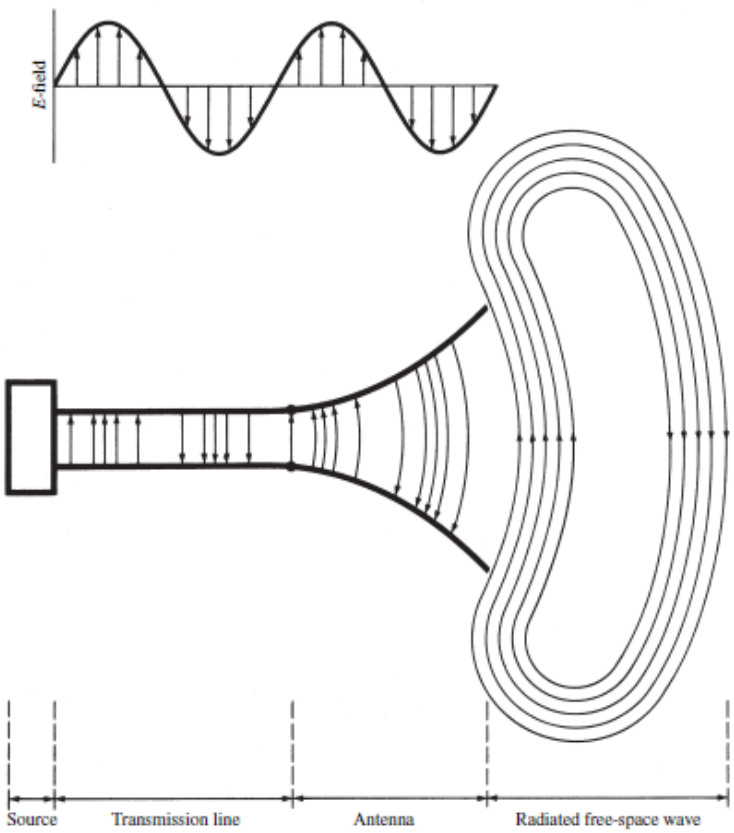

Figure 1: Antenna as a transition device [5].

Antennas are currently used in multiple applications like cellular phones, GPS television, vehicles, radar, satellites, WiFi, Bluetooth technology, RFID devices, WiMAX, etc [18]. Nevertheless, as the spread and usage of antennas keep growing, so do the constraints and requirements of the communication systems. The engineering of better

and more efficient antennas for these systems is essential for the expansion and effectiveness of tomorrow's communications.

To make the analysis and modelling of antennas easier to understand and predict, several numerical methods have been developed. These will be addressed in section 2.2 for microstrip antennas in particular.

2.1 Figures of merit

The antenna performance can be rated according to its main parameters. Depending on the application, some may be more relevant than others and therefore more crucial to enhance in order to have a better antenna for said application.

Radiation pattern

An antenna's radiation pattern is essentially a graphical representation of its radiation properties in the far-field region, as a function of the direction. These properties include power flux density, radiation intensity, field strength, directivity, phase, and polarization [5].

Some of the most common patterns are shown in Figure 2:

- Isotropic, when the antenna radiates equally in all directions. This is a hypothetical ideal concept.
- Directional, when the antenna radiates more effectively in some direction than in the others
- Omnidirectional, when in a certain plane the radiation pattern is constant and in an orthogonal plane is directional

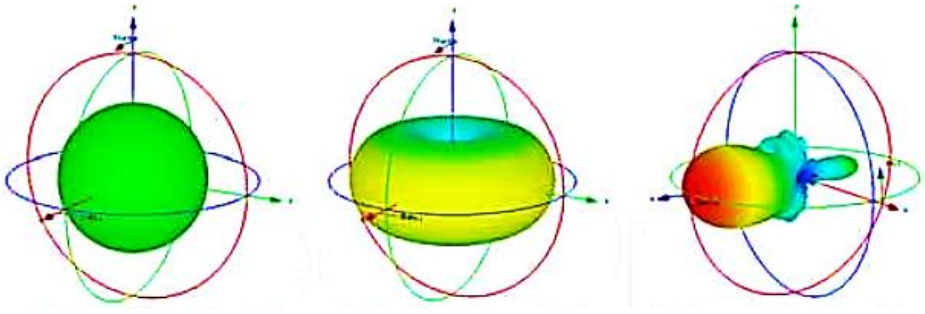

Figure 2: Radiation pattern examples: isotropic, omnidirectional, and directional [19].

Directivity

The directivity of an antenna is defined as the ratio of radiation intensity in a given direction to the radiation intensity of an ideal isotropic antenna, which radiates equally in all directions, radiating the same power. By taking U as the radiation intensity and U_0 as the radiation intensity of an isotropic source, the directivity will be:

$$D(\theta,\phi) = \frac{U(\theta,\phi)}{U_0} = \frac{4\pi U(\theta,\phi)}{P_{rad}} \tag{2.1}$$

Where P_{rad} is the total radiated power.

Gain

The gain is a similar concept to the directivity but takes into consideration the antenna's efficiency which accounts for the losses that occur in the antenna. This means that it is the ratio of radiation intensity in a given direction to the radiation intensity of an ideal isotropic antenna, which has no losses associated, fed with the same power. Thus,

$$G(\theta,\phi) = \frac{U(\theta,\phi)}{U_0} = \frac{4\pi U(\theta,\phi)}{P_{in}} \tag{2.2}$$

Bandwidth

The bandwidth of a given antenna is the range of frequencies in which the antenna's characteristics are within a certain limit. For example, taking into consideration the S_{11} parameter, which represents how much power is reflected from the antenna, the bandwidth is defined as the frequency range for which it is below -10dB. This is analogous with other parameters - such as gain, side lobe level, radiation efficiency, polarization, beamwidth, etc – by having defined limits within which the parameter value is acceptable. If an antenna has a large bandwidth, it is labeled broadband, and if it has a small bandwidth, it is labeled narrowband [5].

The quality (Q) factor is a popular way to quantify an antenna's bandwidth. This factor is defined as the ratio of power stored in the reactive field to radiated power. Thus, it is a measure of the antenna's radiation efficiency. The higher the Q, the less bandwidth the antenna has.

Polarization

The polarization of an antenna in each direction is the same as that of the electromagnetic wave that it produces when it is radiating. In a linearly polarized antenna, the electric field remains oriented along a straight line throughout time. In an elliptically polarized antenna, the electric field traces an elliptical shape. In a circularly polarized antenna, the electric field traces a circle as a function of time; this can happen with clockwise rotation and therefore it is Right-Hand Circular Polarization (RHCP), or it can happen counterclockwise and in that case it is Left-Hand Circular Polarization (LHCP). These three polarization types (linear, elliptical, and circular) can be observed in Figure 3.

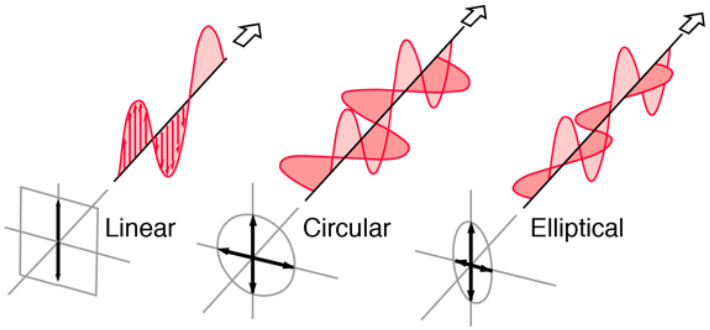

Figure 3: Types of polarizations [20].

This also leads to an important concept of Axial Ratio, which is defined as the ratio of the major axis to the minor axis.

For a receiving antenna to be able to retrieve the maximum amount of energy from an electromagnetic wave arriving from a source antenna, it should have a polarization compatible with the polarization of the wave (for example for receiving a vertically polarized wave, one should use a vertically polarized antenna in the same direction). When this doesn't happen there will be less energy received.

Input impedance

The input impedance is the impedance the antenna presents at its terminals. To achieve maximum power transfer to/from the antenna, the input impedance must match the antenna feed. This parameter is frequency dependent and therefore the feed network will be adapted to the antenna at a specific frequency (or band) for which it was designed.

2.2 Types of antennas

Antennas can take several forms. In this section, an overview of some of them will be given, emphasizing those more relevant to the purpose of this dissertation.

Wire antennas

Wire antennas are constituted by a conductive wire in which an electrical current flows. This wire can be straight such as the dipole, a loop (circular, square, ellipse, rectangle...) or a helix. Wire antennas are very versatile, cheap, and simple to build and analyze, which explains why they are used in diverse applications such as automobiles ships, aircrafts, buildings, etc. Some wire antenna configurations can be seen below in Figure 4.

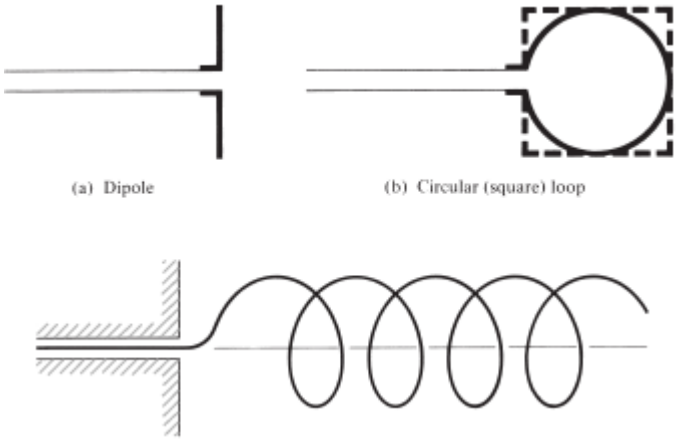

Figure 4: Examples of wire antennas [5].

Aperture antennas

Aperture antennas are formed by an aperture where an electromagnetic field distribution exists. They are most common at microwave frequencies and may take the form of a waveguide or a horn with a square, rectangular, circular, or elliptical aperture. Some examples of aperture antennas are shown in Figure 5.

The horn antenna is often used to feed reflectors and lenses, as well as a standard for calibration and gain measurements. It is a versatile antenna, easy to build and has large gain, making it preferable for applications such as astronomy and satellites.

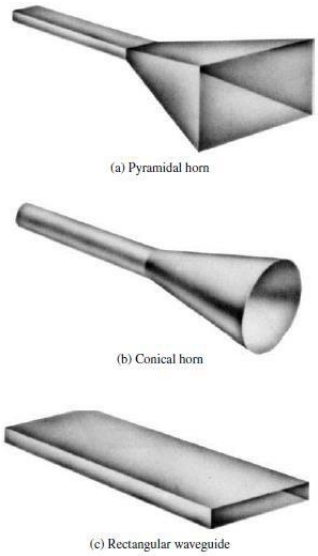

Figure 5: Examples of aperture antennas [5].

Microstrip antennas

Microstrip antennas have the advantage of being low-profile, simple to manufacture, inexpensive, robust when mounted on rigid surfaces, and versatile. This makes them prone to be used in aircraft, spacecraft, satellite, and missile applications where these characteristics are valued. They can be integrated into circuits easily and can be designed to fulfill various requirements.

On the other hand, microstrip antennas have low efficiencies and power, high Q (which makes them more sensitive to frequency variations), low polarization purity and scan performance, spurious feed radiation and narrow bandwidth. However, there are techniques that can be employed to avoid these problems: for example, for wider bandwidths, multiple patches can be stacked, make use of a thicker substrate, sequentially rotate the elements, etc.

Microstrip antennas consist of a metallic patch above a dielectric substrate, with a ground plane underneath. This patch can take several shapes such as rectangular, circular, square, etc.

There are mathematical methods used for the analysis and modelling of microstrip antennas. The most popular are the Transmission-Line, Cavity and Full Wave models [5]. The Transmission-Line Model is the easiest but the least accurate and least versatile. It treats the patch as an array of two radiating slots (see Figure 9). The Cavity Model is more versatile than the former but also more complex. It treats

the dielectric substrate as a cavity bounded by electric conductors and magnetic walls. The Full-Wave Models are very accurate and versatile but the most complex.

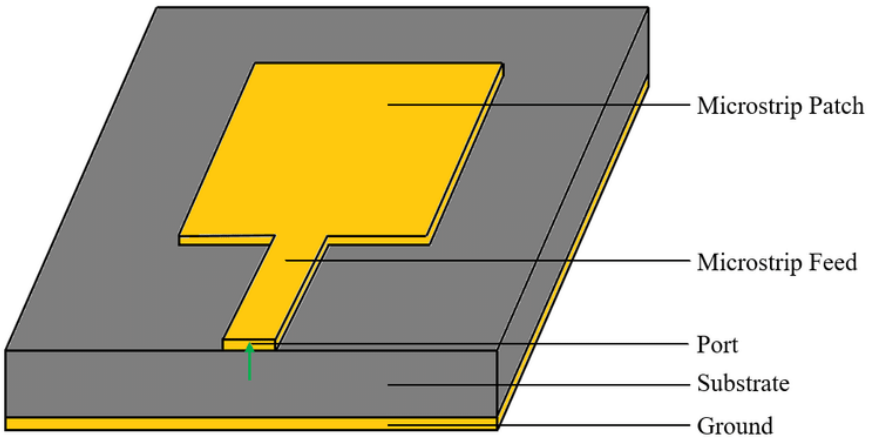

Figure 6: Basic structure of a microstrip antenna [21].

The antenna may be excited using several methods. Variations of these can also be used and adapted to particular requirements of a given application.

- **Coaxial Probe**, shown in Figure 7, is one of the simplest. The patch can be fed using a coaxial probe with the center pin soldered to the patch and the outer conductor to the ground. The location of the probe should be at a point which the patch has the same impedance as the probe (50 Ω) to prevent losses due to mismatch.

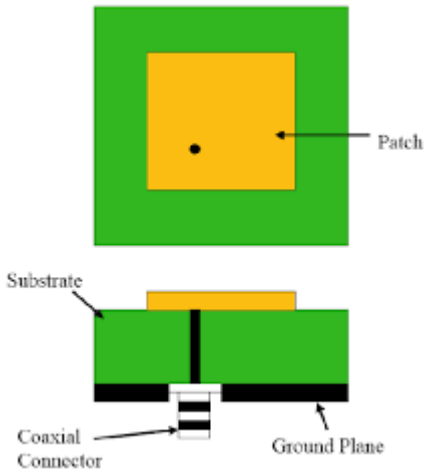

Figure 7: Coaxial probe feed of a microstrip patch antenna.

- **Microstrip Line** – the patch can be connected directly to a microstrip transmission line, as shown in Figure 6. The matching of this microstrip line to

the patch can be accomplished in mainly two ways: using quarter-wavelength transformers to achieve the required impedance (Figure 8) or making an inset cut to the patch (Figure 9).

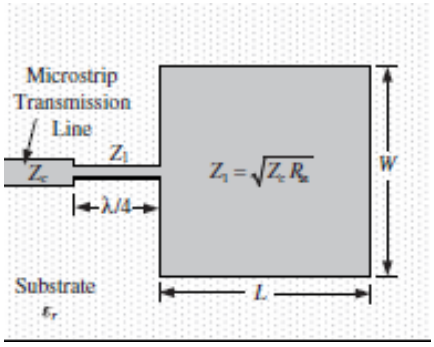

Figure 8: Microstrip Line Feed with λ/4 transformer [5].

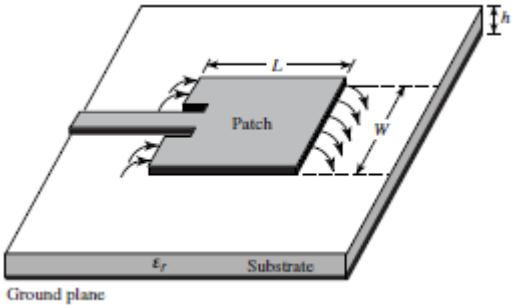

Figure 9: Microstrip Line Feed with recessed line [5].

- **Proximity-coupled Microstrip Line** – by placing an open-ended microstrip line near the patch, the patch can be fed through proximity coupling (Figure 10). The Microstrip Transmission Line can be placed underneath the patch, at the location in which the patch has the same impedance as the line. The line can also be placed in parallel and very closed to the edge of the patch. These methods steer clear of any soldering connection, which can attain better reliability.

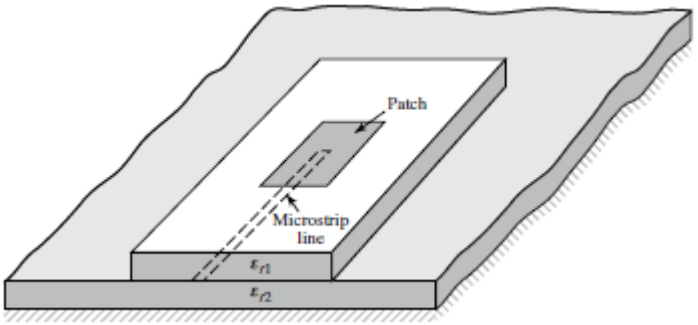

Figure 10: Proximity-coupled Microstrip Line feed [5].

- **Aperture-Coupled Microstrip Line** – Similarly to the proximity coupled feed, an open-ended microstrip line can be placed on one side of the ground plane to feed a patch on the other side of the ground plane, which contains a slot (Figure 11). In addition to the other parameters that are common to other configurations (dielectric constant, patch shape and size, feed line length and

width…), the slot shape, size and position also has a great impact in the performance of these antennas. Some of the most popular slot shapes are rectangular, H shape, bowtie, dogbone, hourglass… In [22], Pozar details the effects each of these parameters has in the antenna's operation.

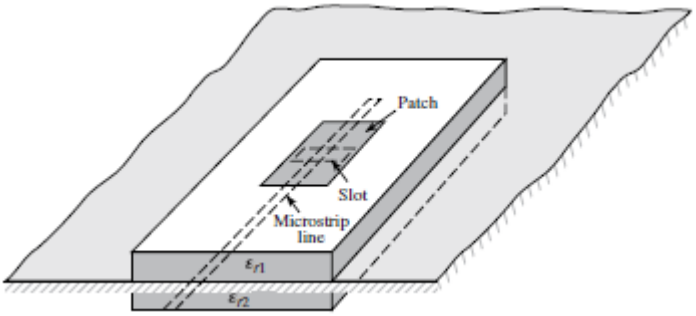

Figure 11: Aperture-Coupled Microstrip Line feed [5].

This configuration has the advantage of achieving higher bandwidths and reducing the leakage radiation from the lines interfering with the patch radiation.

Circular Polarization techniques

Microstrip antennas usually radiate linearly polarized waves by default. However, some adjustments may be made to ensure they become circularly polarized. Circularly polarized antennas are useful because it ensures more flexibility in the relative positioning of the antennas (source and receiver).

Circular polarization can be accomplished by having two orthogonal modes excited with 90º phase difference between them. This can be achieved by either modifying the shape of the patch or having at least two feeds (as shown in Figure 12). When two feeds are used, they must have the same amplitude and a 90º phase difference between them. When geometrical deformation is used, with a single feed, a slot or segment of the patch is truncated in order to separate the generated mode into two orthogonal modes [23]. The position of the feed will determine whether the circular polarization is right or left.

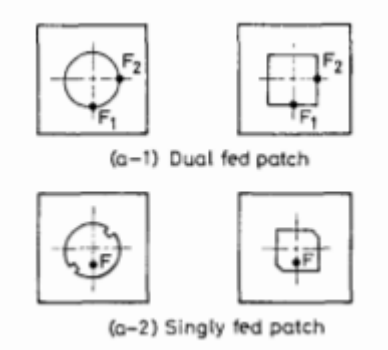

Figure 12: Examples of circularly polarized microstrip antennas [23].

Furthermore, in order to achieve the dual feed with equal amplitude and 90º phase difference, a 3dB hybrid can be employed. This hybrid ensures that one of the output ports is in phase with the input and the other has a 90º phase difference, in addition to both having a 3dB loss from the input. By feeding one input port or the other, one can choose if the circular polarization is oriented left (LHCP) or right (RHCP).

In place of a 3dB hybrid, a simple offset line can also be implemented (Figure 13), ensuring the proper phase difference. However, while the use of a hybrid increases complexity, it also allows the possibility of changing from LHCP to RHCP (and vice-versa) by simply switching the input port.

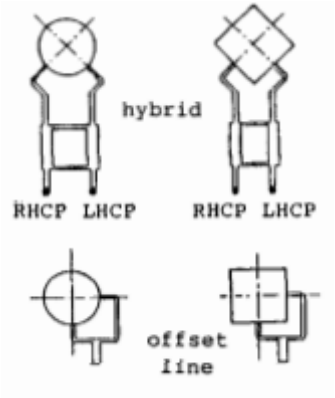

Figure 13: Dual fed CP patches [23].

2.3 Antenna arrays

For certain applications, a single antenna element may not be able to achieve the required radiation characteristics. In these cases, several antennas may be aggregated into arrays, some examples are shown in Figure 14. An array is a geometrical arrangement of several identical antennas. When the array elements are placed along

an axis, it is labeled a linear array; when they are placed along a plane, it is labeled a planar array; and when they are placed along a circumference it is labeled a circular array.

Similarly, to individual elements, the arrays also need to be designed so as to achieve the requirements of the system, for example the radiation from all the elements adding up in a desired direction and cancelling out in another. This can be useful to separate users in a cellular system, improve the systems performance in terms of error rate and reduce the interference between terminals, by directing the main lobe towards the user and nulls towards of the interference. There are several variables that affect the array's performance, such as type of feed (series or parallel), number of layers (single or multiple), substrate thickness, dielectric constant, array size, patch shape and spacing.

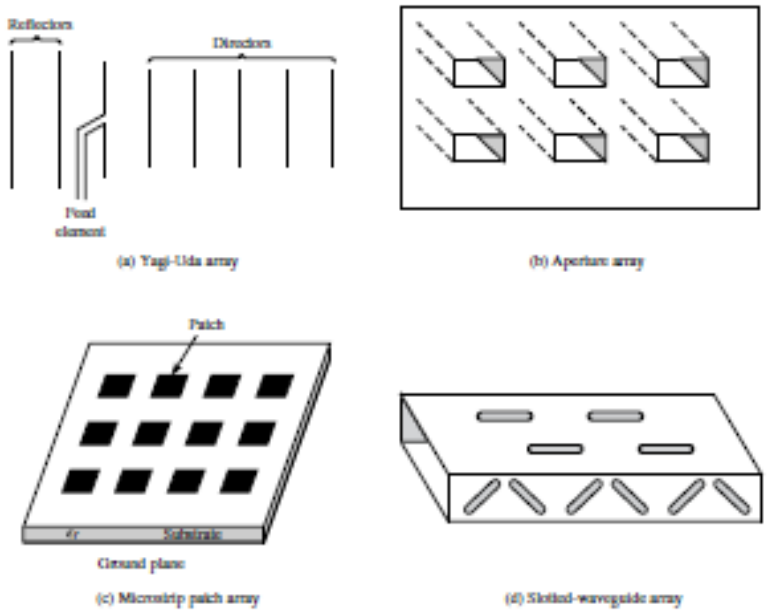

Figure 14: Antenna array examples [5].

While it is possible to build arrays of different antenna types, microstrip antennas are very popular in array configurations due to the ease of integration in arrays and low fabrication cost [24].

3 Design and simulations

To have a first design to simulate and tune the dimensions of the antennas, some approximate equations were used for the calculation of these parameters. Firstly, the calculation of the patch width is done using the expression [5]:

$$W = \frac{c}{2f_r}\sqrt{\frac{2}{\varepsilon_r + 1}} \tag{3.1}$$

In the Transmission Line Model, fringing makes the line look wider electrically compared to its physical dimensions. Because some waves travel in the substrate and some in the air, the effective dielectric constant will be somewhat smaller than the dielectric constant of the substrate [5].

$$\varepsilon_{reff} = \frac{\varepsilon_r + 1}{2} + \frac{\varepsilon_r - 1}{2}\frac{1}{\sqrt{1 + 12\frac{h}{W}}} \tag{3.2}$$

Due to the fringing effect, the patch has an extended effective length. The calculation of the extension ΔL on each side of the patch is done with the following expression:

$$\frac{\Delta L}{h} = 0.412\frac{(\varepsilon_{reff} + 0.3)\left(\frac{W}{h} + 0.264\right)}{(\varepsilon_{reff} - 0.258)\left(\frac{W}{h} + 0.8\right)} \tag{3.3}$$

The real length of the patch is then

$$L = \frac{c}{2f_r\sqrt{\varepsilon_{reff}}} - 2\Delta L \tag{3.4}$$

Before starting the design of this antenna, several patch antenna configurations were simulated to get acquainted with the various feeding methods, patch shapes and slot shapes (in the aperture coupled feed). The first antennas were modelled for 2.4GHz due to the simplicity to design for lower frequencies, and the latter antennas then transformed for 20GHz. These designs can be seen in the figures below:

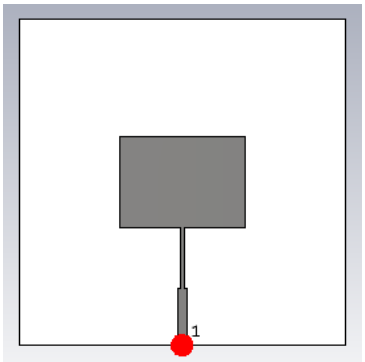

Figure 15: Microstrip line fed rectangular patch (2.4GHz), with quarter-wavelength transformer.

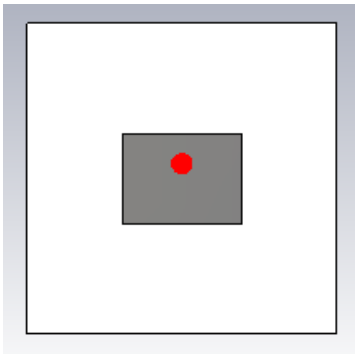

Figure 16: Coaxial fed rectangular patch (2.4GHz).

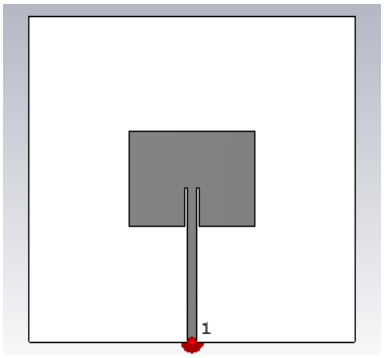

Figure 17: Microstrip line fed rectangular patch (2.4GHz), with inset feed.

For these antennas, the dielectric substrate used for the simulations was the FR-4. This material has a dielectric constant of ε = 4.3 and was simulated as loss free. It has a substrate thickness of h = 1.6 mm.

Each of these antennas was designed by calculating the theoretical dimensions first and then using simulation to fine-tune these dimensions for the desired operating frequency. For this purpose, the Smith Chart is a great tool to allow insight into which part (imaginary or real) of the antenna's impedance is still not matched and therefore which dimension should be changed to achieve impedance matching (as some parameters have more influence in the resistance and some in the reactance of the antenna).

For the structure in Figure 15 the dimensions are shown in Table 1.

Parameter	**Value (mm)**
Patch length (L)	28.7
Patch width (W)	38.39
Length of the λ/4 transformer (L_transf)	18.51
Width of the λ/4 transformer (W_transf)	0.05
Width of 50Ω line (W0)	3.07

Table 1: Dimensions of microstrip line fed rectangular patch (2.4GHz), with quarter-wavelength transformer.

For this antenna, the following results were obtained:

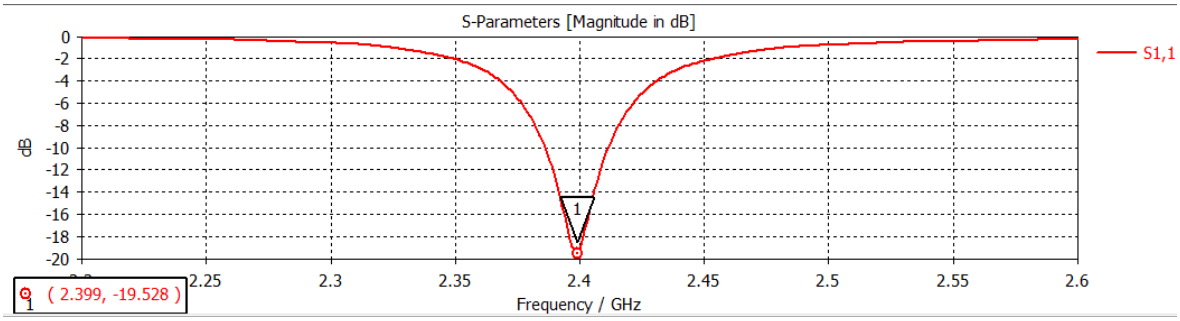

Figure 18: S_{11} of the microstrip line fed rectangular patch with quarter-wavelength transformer.

The S_{11} parameter has a value of -19.5dB at 2.4GHz, which is the desired operating frequency. To achieve this, the use of the Smith Chart for the matching was essential (Figure 19). The length of the patch was adjusted until the desired operating frequency was achieved and the length and width of the quarter-wavelength transformer tuned until the antenna was matched to the 50Ω characteristic impedance of the system.

Figure 19: Smith Chart representation of the S_{11} of the microstrip line fed rectangular patch with quarter-wavelength transformer.

Ideally, the Smith Chart would show the impedance point being at the center of the chart at the operating frequency, meaning the antenna is impedance matched at that frequency. As shown in Figure 19 the antenna has an impedance of $(57.2 - 8.7i)\ \Omega$, which is close to the center of the chart (50Ω) as desired.

For the structure in Figure 16, the dimensions are shown in Table 2.

Parameter	Value (mm)
Patch length (L)	28.9
Patch width (W)	38.4
Position of the coaxial probe (Yf)	4.8

Table 2: Dimensions of the coaxial fed rectangular patch (2.4GHz).

For this antenna, the S_{11} obtained is depicted below:

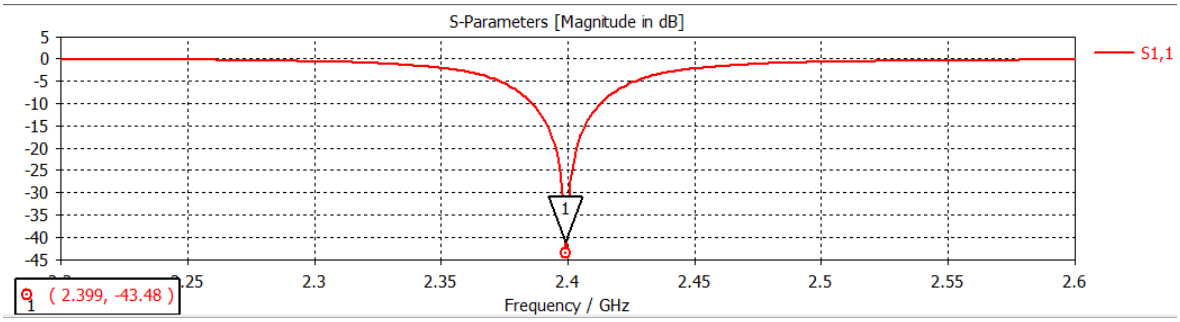

Figure 20: S_{11} of the coaxial fed rectangular patch.

The S_{11} of the coaxial fed antenna (Figure 20) has a value of -43.5dB at 2.4GHz, which is the desired operating frequency. To achieve this frequency, the length of the patch was adjusted and the position of the coaxial feed, which is centered in the patch, changed until the matching was verified. For this purpose, the Smith Chart (Figure 21) was used to have information regarding the antenna's impedance at the operating frequency.

Figure 21: Smith Chart representation of the S_{11} of the coaxial fed rectangular patch.

As can be seen in Figure 21, the antenna is matched to 50Ω at 2.4GHz, having an impedance of $(50.3 + 0.6i)\ \Omega$.

For the structure with the inset feed (Figure 17), the dimensions are shown in Table 3.

Parameter	Value (mm)
Patch length (L)	29.2
Patch width (W)	38.39
Gap between line and patch (Δ)	0.8
Inset portion of line (Y0)	12
Width of 50Ω line (W0)	3.07

Table 3: Dimensions of the microstrip line fed rectangular patch (2.4GHz), with inset feed.

This antenna presented the following results:

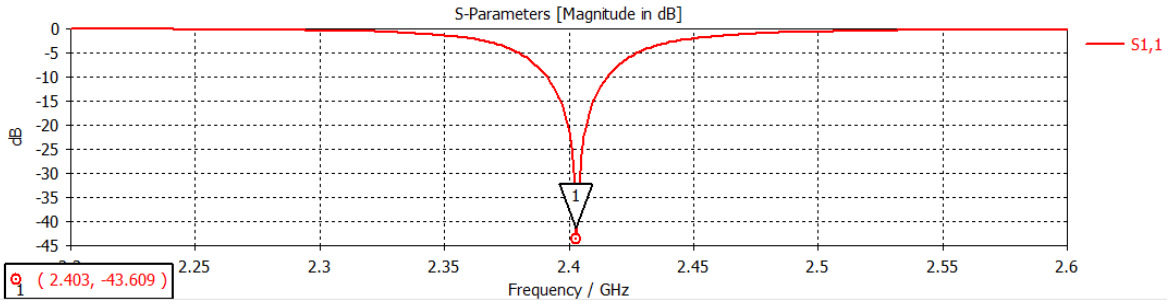

Figure 22: S_{11} of the antenna with inset feed.

The antenna with recessed microstrip line feed presented an S_{11} value of -43.6dB at the target operating frequency of 2.4GHz. To achieve this operating frequency, the length of the patch was adjusted, and the length of the inset feed changed until the matching was verified, using the Smith Chart representation of the impedance (Figure 23).

Figure 23: Smith Chart representation of the S_{11} of the antenna with inset feed.

Once again, Figure 23 shows the antenna is matched to 50Ω at 2.4GHz, having an impedance of $(49.9 - 0.7i)\ \Omega$.

The first structures to be designed were the simplest, with direct contact feeding methods. Then, the more complex structures, with coupling feeding methods were developed. Note that the separation of the several layers is only for clarity, in reality all the layers are together. At this point, the dielectric substrate was changed to Rogers RO4350B. This material has a dielectric constant of ε = 3.66 and electric loss tangent of tan(δ) = 0.0037. The dimensions are substrate thickness of h = 0.76 mm and copper thickness of t = 17µm.

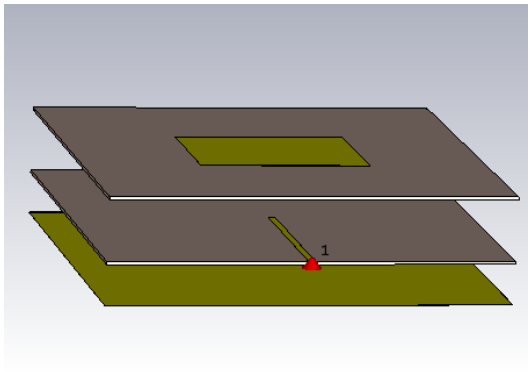

Figure 24: Proximity coupled line fed rectangular patch (2.4GHz).

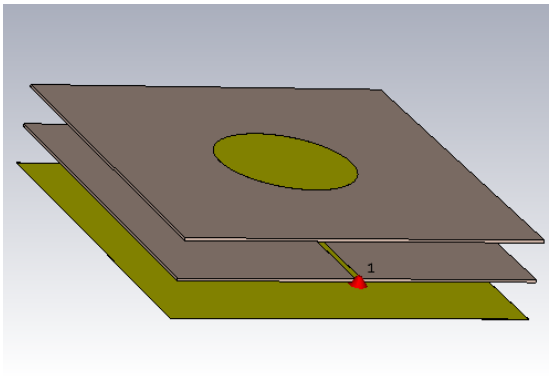

Figure 25: Proximity coupled line fed circular patch (2.4GHz).

Regarding the structure of Figure 24, the proximity coupled line fed rectangular patch antenna, the dimensions are presented below in Table 4.

Parameter	Value (mm)
Patch length (L)	31.8
Patch width (W)	41.8
Portion of line under patch (Ls)	13
Width of 50Ω line (W0)	1.7

Table 4: Dimensions of the proximity coupled line fed rectangular patch (2.4GHz).

For this antenna, the S_{11} results obtained are shown below:

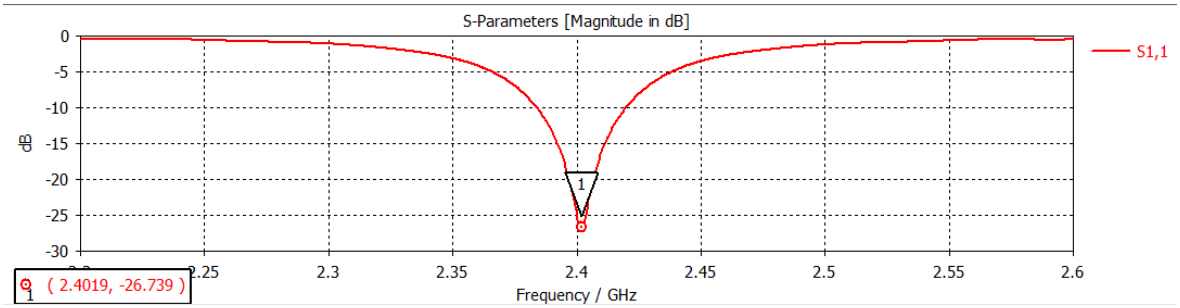

Figure 26: S_{11} of the proximity coupled line fed rectangular patch.

At 2.4GHz, the S_{11} (Figure 26) has a value of -26.7dB. The length of the patch was manipulated to achieve the desired frequency and the length of the feed line adjusted until the antenna was matched to the impedance of the system (50Ω), using the Smith Chart to simplify this process (Figure 27).

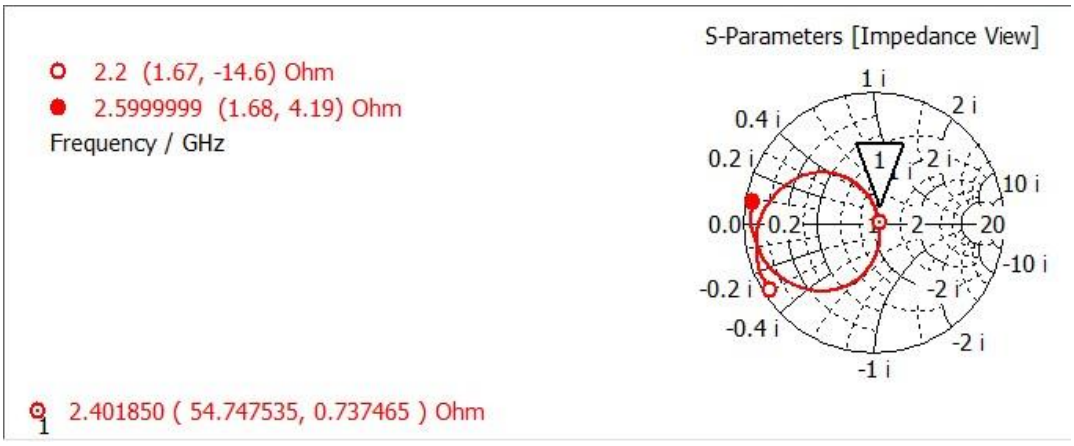

Figure 27: Smith Chart representation of the S_{11} of the proximity coupled line fed rectangular patch.

The figure above (Figure 27) shows the antenna is matched to 50Ω at 2.4GHz, having an impedance of $(54.7 - 0.7i)\ \Omega$.

After, the same structure with a circular patch was designed (Figure 25). Its dimensions are shown in Table 5.

Parameter	Value (mm)
Patch radius (a)	18.6
Portion of line under patch (Ls)	4.2
Width of 50Ω line (W0)	1.7

Table 5: Dimensions of the proximity coupled line fed circular patch (2.4GHz).

The results obtained for this antenna are below:

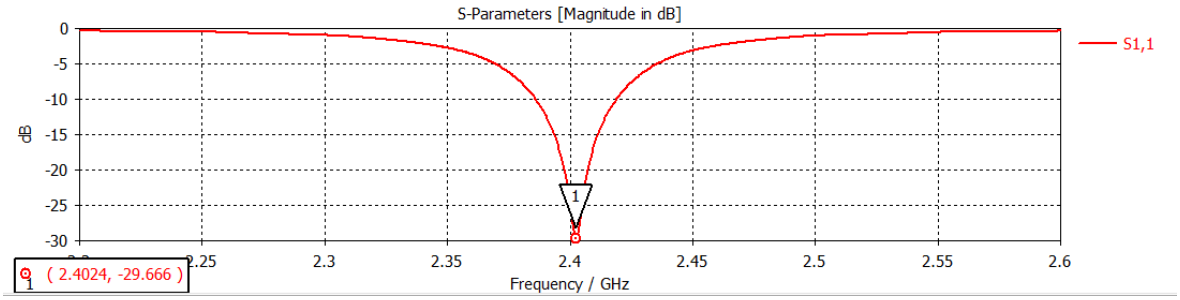

Figure 28: S_{11} of the proximity coupled line fed circular patch.

The S_{11} (Figure 28) at 2.4GHz is -29.7dB. The radius of the patch was tuned to achieve the desired operation frequency and the length of the feed line adjusted until the antenna was matched to the impedance of the system (50Ω), using the Smith Chart to simplify this process (Figure 29).

Figure 29: Smith Chart representation of the S_{11} of the proximity coupled line fed circular patch.

The Smith Chart (Figure 29) shows the antenna is matched, having an impedance of $(47.7 + 2.3i)\Omega$.

Then, the aperture coupled line fed antennas were also tested, with circular, rectangular, and square patches and with three slot shapes: rectangular, H and bowtie.

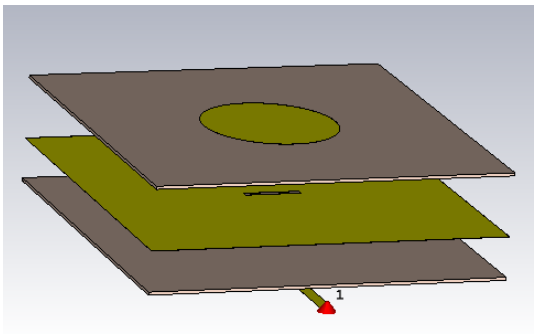

Figure 30: Aperture coupled line fed circular patch (2.4GHz) with rectangular slot.

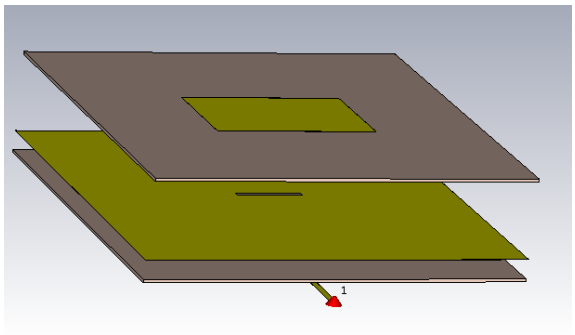

Figure 31: Aperture coupled line fed rectangular patch (2.4GHz) with rectangular slot.

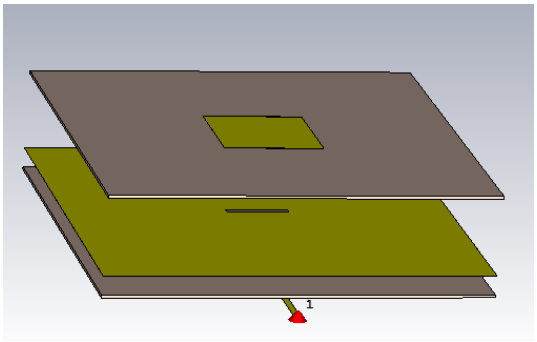

Figure 32: Aperture coupled line fed square patch (2.4GHz) with rectangular slot.

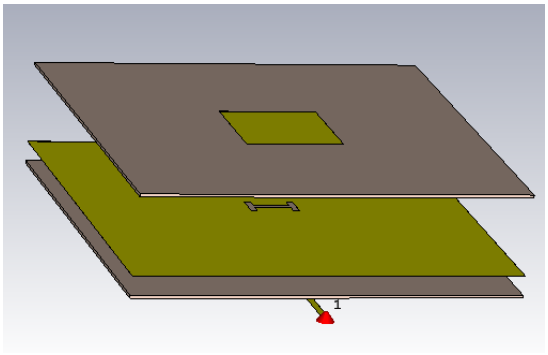

Figure 33: Aperture coupled line fed square patch (2.4GHz) with H slot.

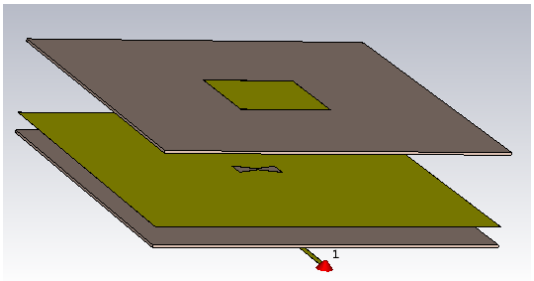

Figure 34: Aperture coupled line fed square patch (2.4GHz) with bowtie slot.

Since the patch had already been calculated, the transmission line must be dimensioned. The feed line should be aligned with the center of the slot and the patch for maximum coupling [22]. Its width defines the characteristic impedance and must match the rest of the system. The impedance is defined to be 50Ω and therefore the width of the line must be *W0 = 1.1 mm*. This width of the feed line affects the coupling to the slot – the thicker the line, the stronger the coupling to the slot. The calculation software *TxLine* is used to reach this result. The length of the part of the transmission

line after the slot, Ls, is usually slightly smaller than $\lambda_g/4$ which has the value $\frac{\lambda_g}{4} = 2.1mm$. It is used to tune the excess reactance of the slot coupled antenna. When the length Ls is reduced, the impedance locus in the Smith Chart representation of the antenna's impedance moves in the capacitive direction (down). This means this length should be adjusted until the impedance is purely real at the design frequency (see Figure 35).

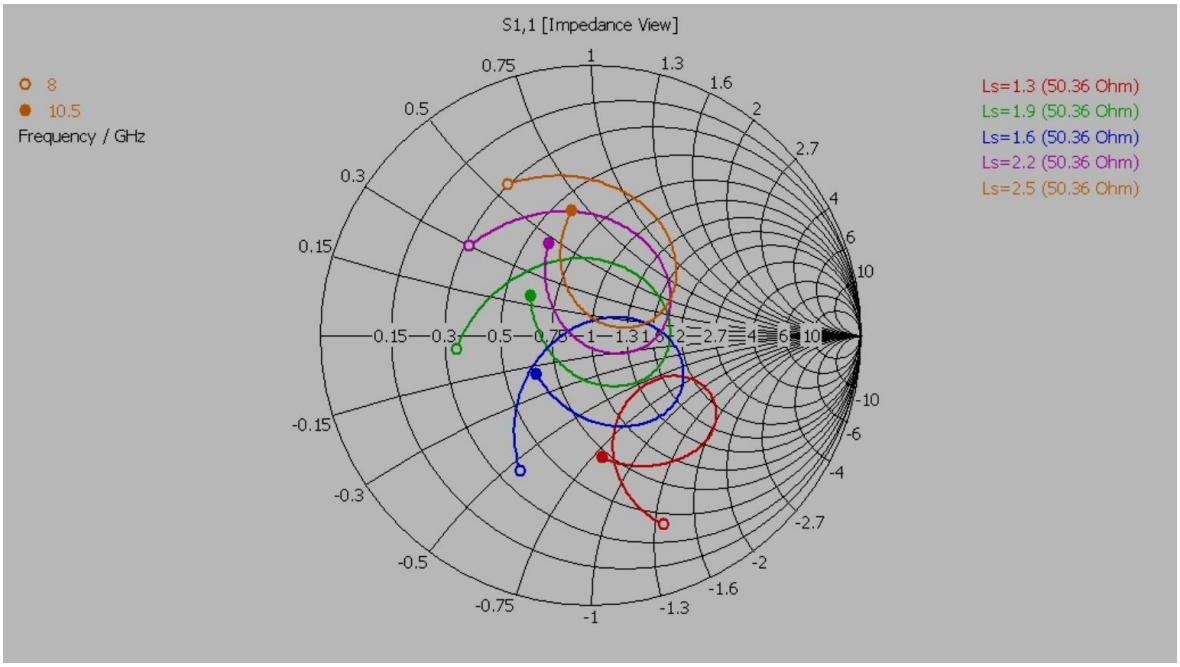

Figure 35: Smith Chart of a parametric analysis of the length of the stub on an aperture coupled antenna [25].

Finally, the dimensions and position of the slot must be calculated. The length of the aperture should be $0.1\lambda < La < 0.2\lambda$, but no larger than required for the impedance matching, and the width about one tenth of the length. The slot length affects the resonant frequency, determines the coupling level and controls the size of the locus in the Smith Chart representation of the antenna's impedance (see Figure 36). Thus, $1.5 < La < 3$ mm and $\mathrm{Wa} = \mathrm{La}/10$.

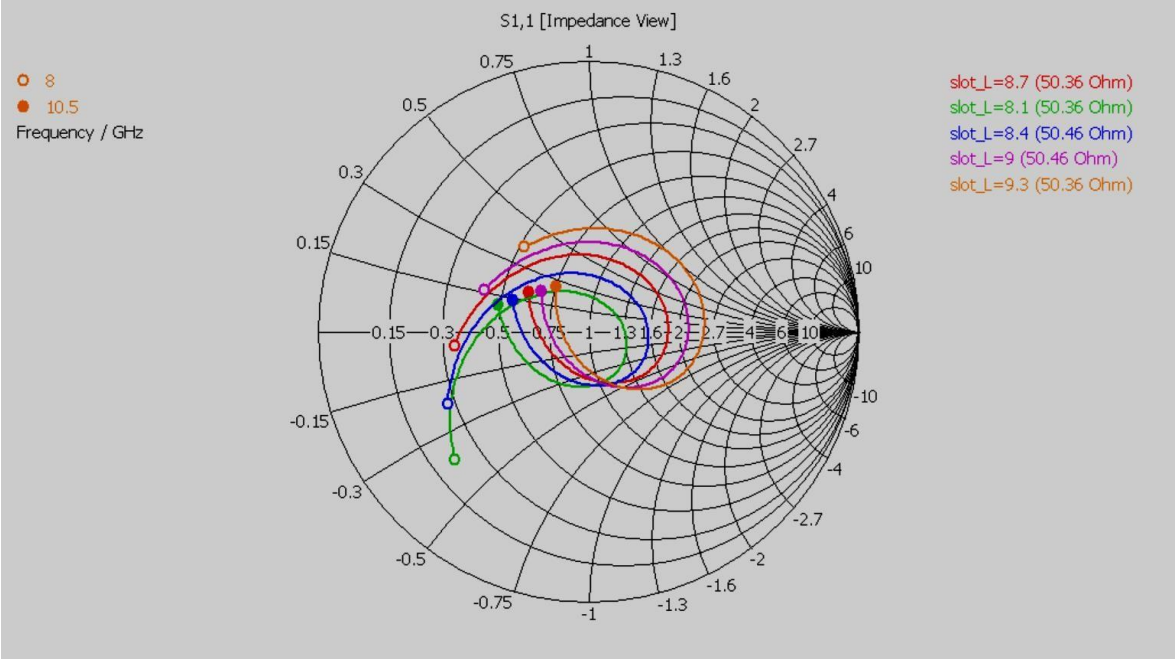

Figure 36: Smith Chart of a parametric analysis of the length of the slot on an aperture coupled antenna [25].

Regarding the antenna of Figure 30, the dimensions are shown in Table 6.

Parameter	**Value (mm)**
Patch radius (a)	16.75
Slot length (La)	14.2
Slot width (Wa)	1.42
Position of slot (Ya)	-5
Portion of line after slot center (Ls)	16
Width of 50Ω line (W0)	1.7

Table 6: Dimensions of the aperture coupled line fed circular patch (2.4GHz) with rectangular slot.

For this antenna, the S_{11} is shown in the following figure:

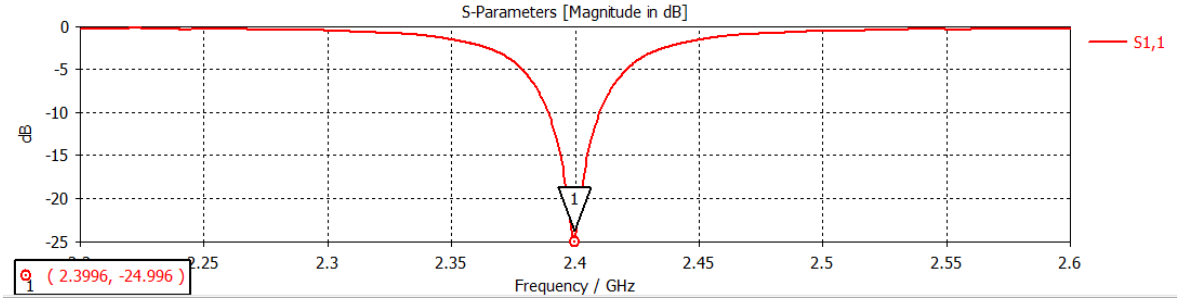

Figure 37: S_{11} of the aperture coupled line fed circular patch with rectangular slot.

The S_{11} (Figure 37) has a value of -25dB at 2.4GHz, which is the desired operating frequency. To achieve this, the use of the Smith Chart for the matching was indispensable (Figure 38). In aperture coupled structures there are many parameters that influence the performance of the antenna and so, after designing the antenna with the theoretical values of the dimensions, only the most relevant parameters were adjusted, leaving those that have less influence in the performance constant. To this purpose, the *parameter sweep* function of CST was employed. The radius of the patch and slot length were adjusted until the desired operating frequency was achieved, and simultaneously the length of the feeding line and the length of the aperture were tuned until the antenna was matched to the 50Ω characteristic impedance of the system.

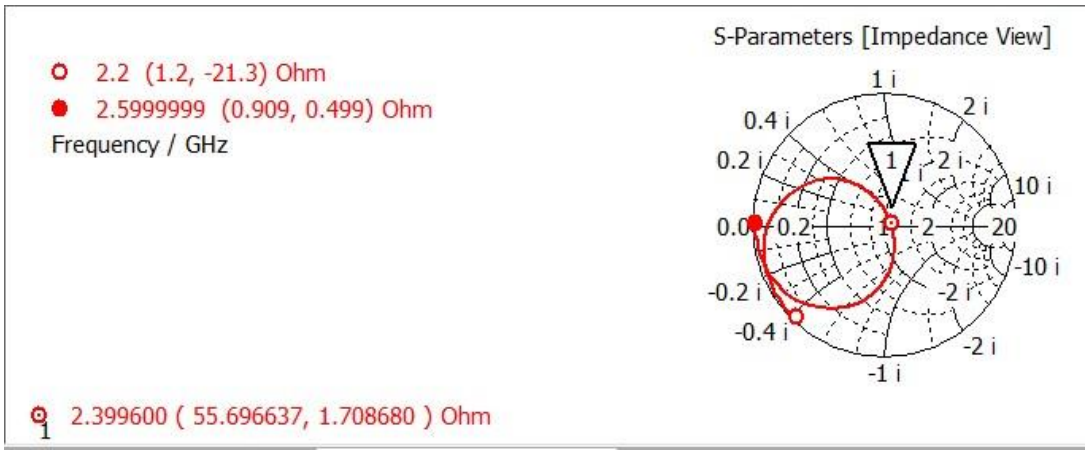

Figure 38: Smith Chart representation of the S_{11} of the aperture coupled line fed circular patch with rectangular slot.

As can be seen in Figure 38, the antenna is matched to 50Ω at 2.4GHz, having an impedance of $(55.7 + 1.7i)\ \Omega$. This tool is fundamental to the design of this type of structure. The length of the feeding line mainly influences the imaginary part of the impedance (reactance), and the size of the slot affects the real part of the impedance and the resonance frequency.

The same structure with a rectangular patch was then simulated (Figure 31). The dimensions for this antenna are shown in Table 7.

Parameter	Value (mm)
Patch length (L)	26.6
Patch width (W)	41.8
Slot length (La)	17.2
Slot width (Wa)	1.72
Position of slot (Ya)	0
Portion of line after slot center (Ls)	17
Width of 50Ω line (W0)	1.7

Table 7: Dimensions of the aperture coupled line fed rectangular patch (2.4GHz) with rectangular slot.

The obtained results are shown below:

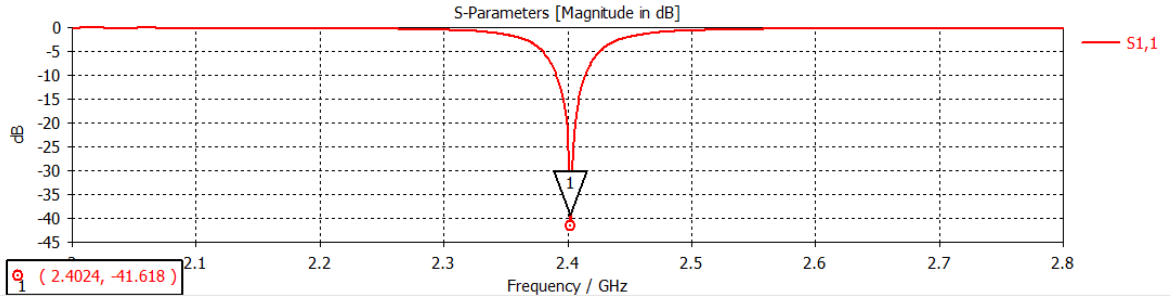

Figure 39: S_{11} of the aperture coupled line fed rectangular patch with rectangular slot.

The rectangular patch with aperture coupled feed presented an S_{11} value of -41.6dB (Figure 39) at the target operating frequency of 2.4GHz. To achieve this operating frequency, the same process as in the previous antenna was used, using the Smith Chart representation of the impedance (Figure 40).

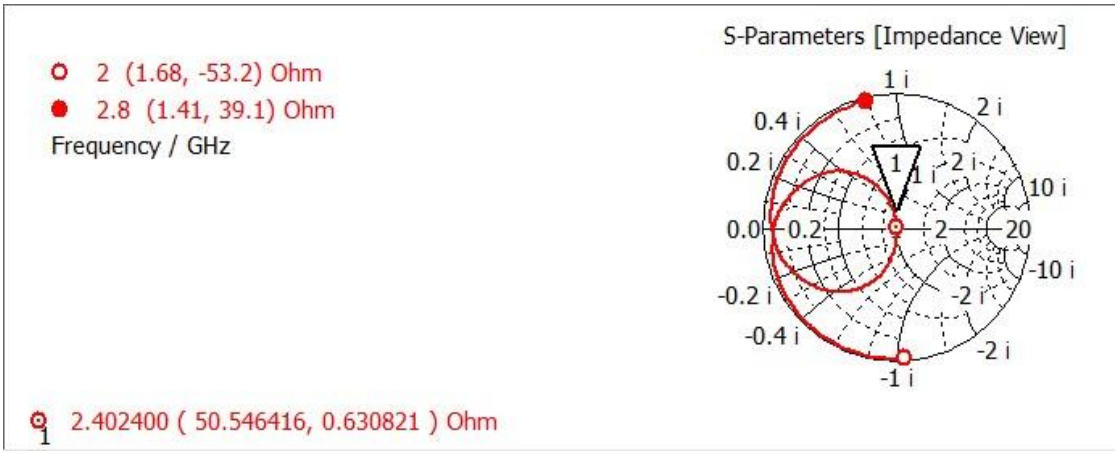

Figure 40: Smith Chart representation of the S_{11} of the aperture coupled line fed rectangular patch with rectangular slot.

The antenna is matched at 2.4GHz, having an impedance of $(50.5 + 0.6i)\ \Omega$. The length of the feeding line mainly influences the imaginary part of the impedance (reactance), and the size of the slot affects the real part of the impedance and the resonance frequency.

Next, the same structure was simulated with a square patch (Figure 32).

Because a square patch is needed, and not a rectangular one, the width of the patch is made to be equal to the length, since it is the latter that defines the resonant frequency.

The dimensions of this antenna are shown in Table 8.

Parameter	**Value (mm)**
Patch length (L)	25.5
Slot length (La)	16
Slot width (Wa)	1.6
Position of slot (Ya)	0.2
Portion of line after slot center (Ls)	16
Width of 50Ω line (W0)	1.7

Table 8: Dimensions of the aperture coupled line fed square patch (2.4GHz) with rectangular slot.

In Figure 41 is the S_{11} result:

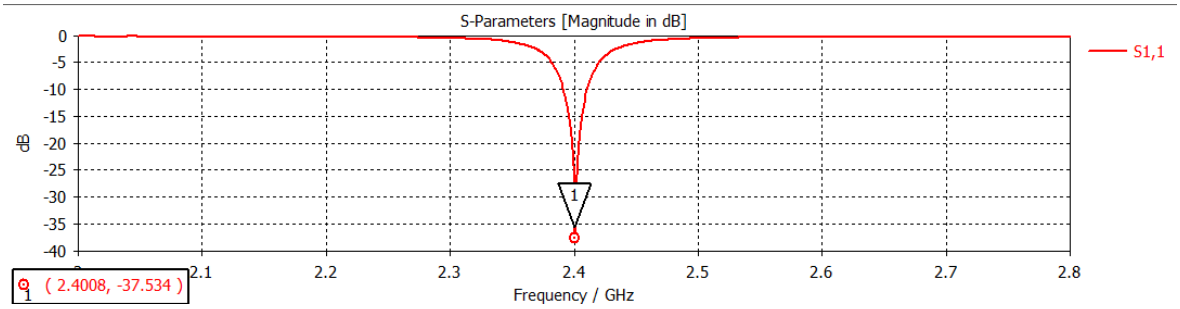

Figure 41: S_{11} of the aperture coupled line fed square patch with rectangular slot.

The square patch with aperture coupled feed presented an S_{11} value of -37.5dB at the target operating frequency of 2.4GHz. To achieve this operating frequency, the same process as in the previous antennas was used, using the Smith Chart representation of the impedance (Figure 42). Taking -10dB as the limit, the bandwidth is approximately 19.2MHz.

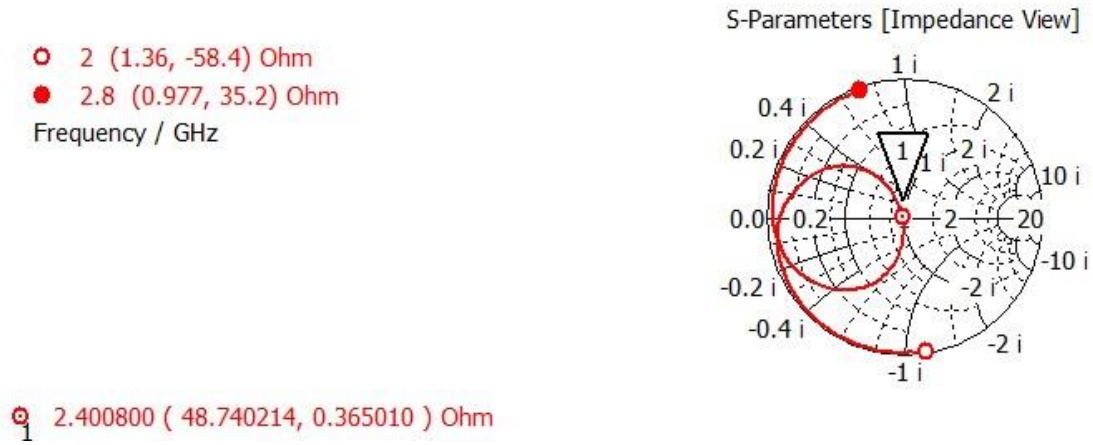

Figure 42: Smith Chart representation of the S_{11} of the aperture coupled line fed square patch with rectangular slot.

The figure above (Figure 42) shows the antenna is matched to 50Ω at 2.4GHz, having an impedance of $(48.7 + 0.4i)\ \Omega$.

Following, the previous structure (aperture coupled line fed square patch with rectangular slot) was designed to replace the slot with an H-shaped slot (Figure 33) and bowtie slot (Figure 34).

The dimensions of the antenna of Figure 33 are shown in Table 9.

Parameter	Value (mm)
Patch length (L)	25.1
Slot length (La)	12.5
Slot width (Wa)	1.6
H slot height (Lh)	6.25
Position of slot (Ya)	1
Portion of line after slot center (Ls)	16
Width of 50Ω line (W0)	1.7

Table 9: Dimensions of the aperture coupled line fed square patch (2.4GHz) with H slot.

The results regarding the S_{11} of the structure with the H slot are shown below:

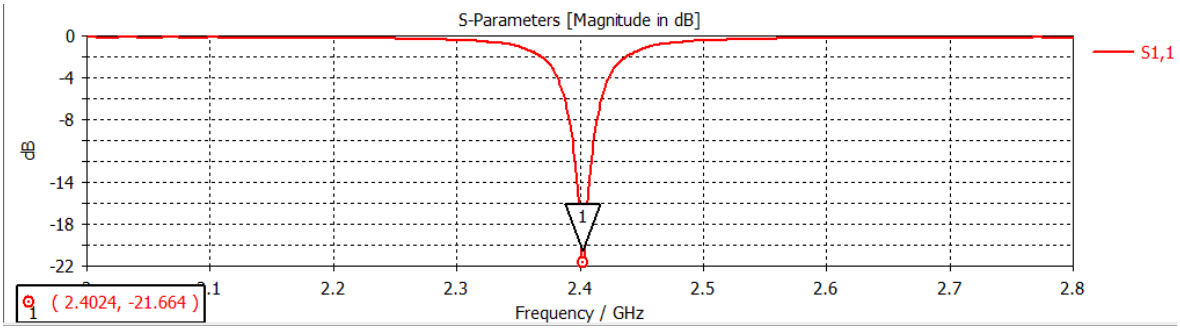

Figure 43: S_{11} of the aperture coupled line fed square patch with H slot.

As shown in Figure 43, the S_{11} has a value of -21.7dB at the target operating frequency of 2.4GHz. Taking -10dB as the limit, the bandwidth is approximately 17.3MHz.

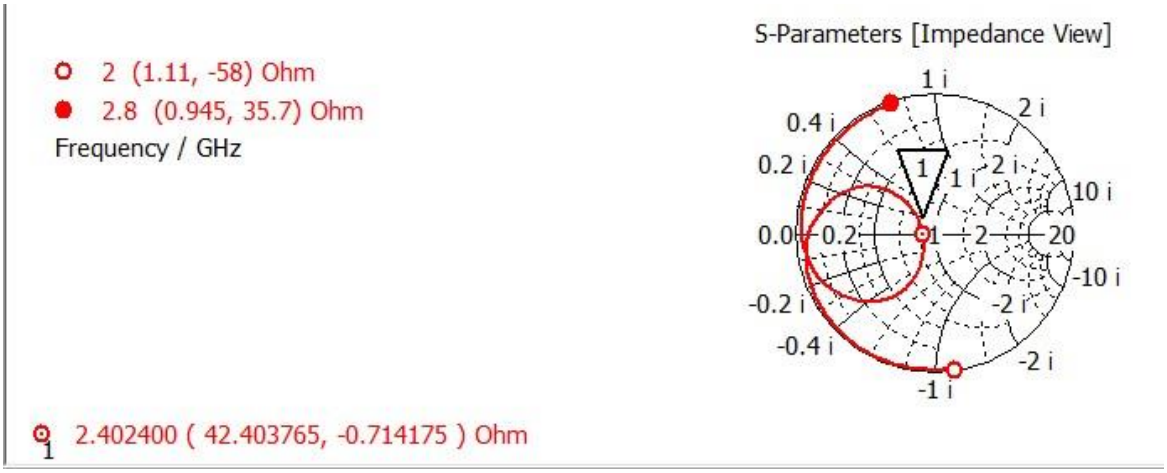

Figure 44: Smith Chart representation of the S_{11} of the aperture coupled line fed square patch with H slot.

The Smith Chart (Figure 44) shows the antenna is matched, having an impedance of $(45.9 + 0.6i)\Omega$.

The dimensions of the antenna of Figure 34 are shown in Table 10.

Parameter	Value (mm)
Patch length (L)	26.2
Slot length (La)	12.5
Bowtie slot outer width (Wa)	5.5
Bowtie slot inner width (Wai)	1
Position of slot (Ya)	0
Portion of line after slot center (Ls)	16
Width of 50Ω line (W0)	1.7

Table 10: Dimensions of the aperture coupled line fed square patch (2.4GHz) with bowtie slot.

For the structure with the bowtie slot, the results are as following:

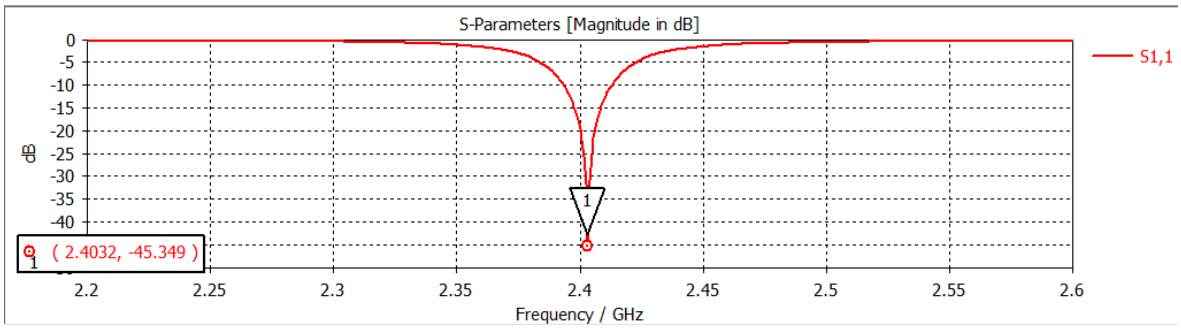

Figure 45: S_{11} of the aperture coupled line fed square patch with bowtie slot.

As shown in Figure 45, the S_{11} has a value of -45.3dB at the target operating frequency of 2.4GHz. Taking -10dB as the limit, the bandwidth is approximately 19.5MHz.

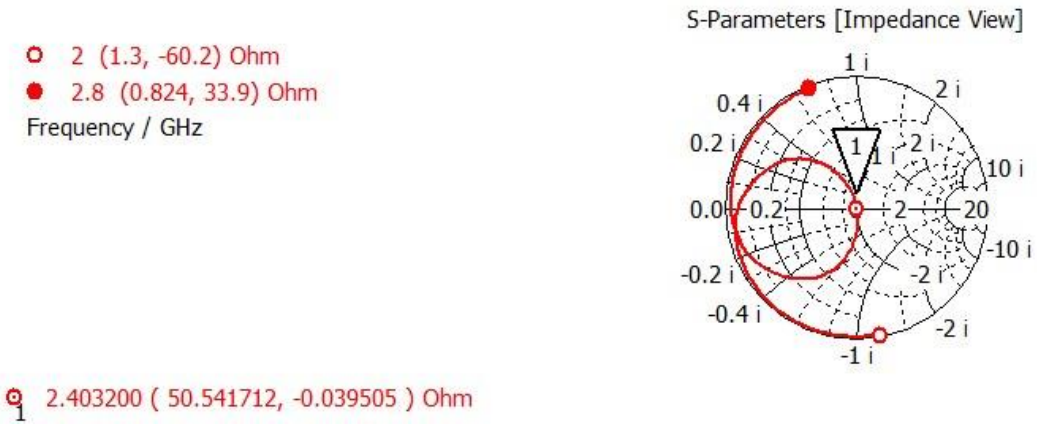

Figure 46: Smith Chart representation of the S_{11} of the aperture coupled line fed square patch with bowtie slot.

The Smith Chart (Figure 46) shows the antenna is matched, having an impedance of $(50.5 - 0.04i)\Omega$.

The aperture coupled structures were then adapted to the operating frequency of 20GHz, to meet the prototype's requirements. From the slot shapes shown above, the one chosen to be used in the prototype was the H shape for improved coupling and convenience, and the patch shape was chosen to be square to simplify the feeding in two orthogonal points later on.

The design of the prototype was completed in several cumulative steps to attempt a more precise and simplified process.

The first step of the design was the modelling of a square microstrip antenna for 20GHz with an aperture coupled feed. In order to design a square patch antenna, the Transmission Line Model was used for the calculations of approximate dimensions.

The dielectric substrate chosen to be used for this project was the Rogers RO4350B due to its availability for use in the prototype, as well as compatibility with the requirements. This material has a dielectric constant of ε = 3.66 and electric loss tangent of tan(δ) = 0.0037. The dimensions are substrate thickness of h = 0.508 mm and copper thickness of t = 17μm. With higher substrate thickness, wider bandwidths and less coupling can be achieved. The dielectric constant affects mainly the bandwidth and radiation efficiency. The same substrate was used for both layers (above and below the ground plane).

3.1 Design of the single-fed patch antenna

The calculated values in Table 11 were the starting point for the CST simulations. The antenna was designed and simulated, and the values adjusted in order to obtain the desired results.

Parameter	Value (mm)
Patch length (L)	2.7
Slot length (La)	1.3
Slot width (Wa)	0.3
H slot height (Lh)	0.9
Position of slot (Ya)	0
Portion of line after slot center (Ls)	0.37
Width of 50Ω line (W0)	1

Table 11: Dimensions of the single-fed patch antenna.

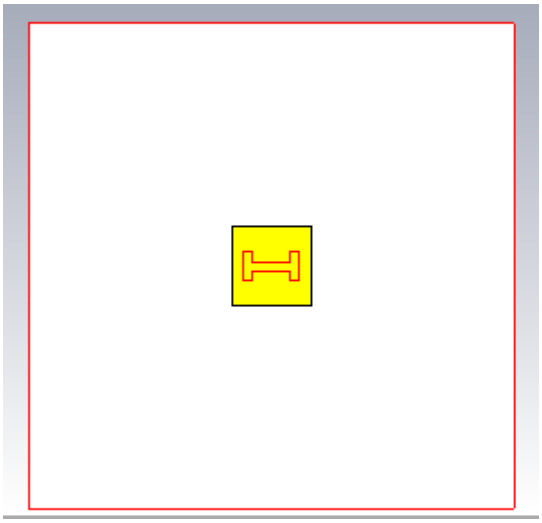

Figure 47: Top view of the single-fed antenna.

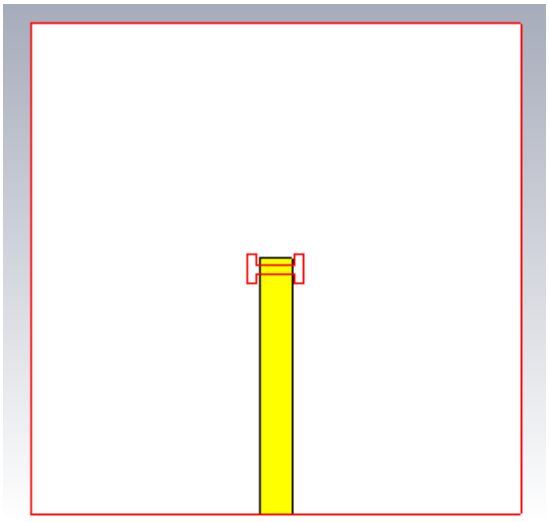

Figure 48: Bottom view of the single-fed antenna.

In Figure 47 and Figure 48 is seen the front and back view of the antenna designed, with the ground plane in red outline (the H in the center is the ground slot). Predominantly, the slot and stub length need to be adjusted for proper matching to the patch.

The main results that need to be taken into consideration are the S_{11} and the gain. The S_{11} represents the reflection coefficient of the antenna. It can be represented in a Smith Chart, which should be matched (≈ 1, at the center of the Smith Chart) at the operating frequency or in a graph of dB in function of frequency, which should be minimum near the operating frequency. The gain can be represented in two 2D graphs or in a 3D graph, with the units being dBi.

Figure 49 and Figure 50 represent the results of the antenna's simulated S_{11}, in rectangular and Smith Chart representation, respectively. The antenna is found to be well matched at the target frequency, 20GHz, with an S_{11} of -31.2dB. Additionally, a bandwidth of about 621MHz can be verified, which corresponds to 3% of the center frequency.

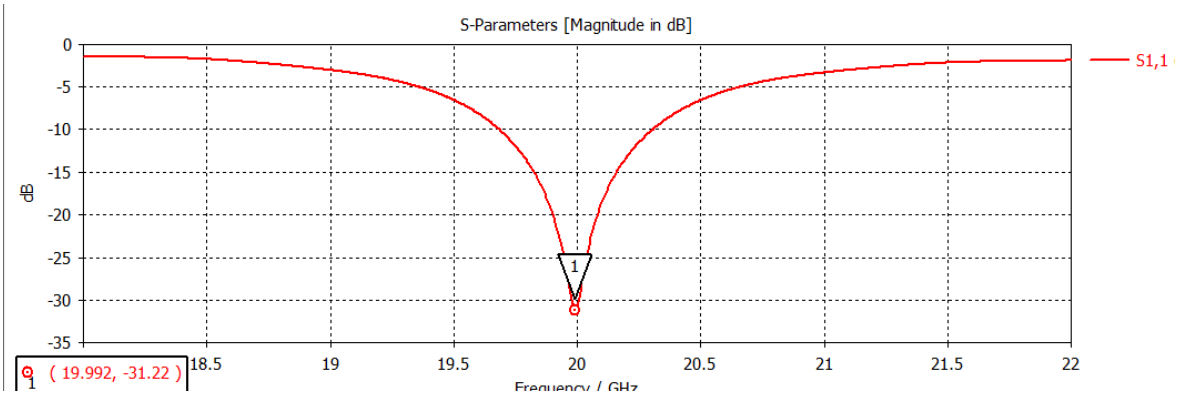

Figure 49: S_{11} in dB of the single-fed antenna.

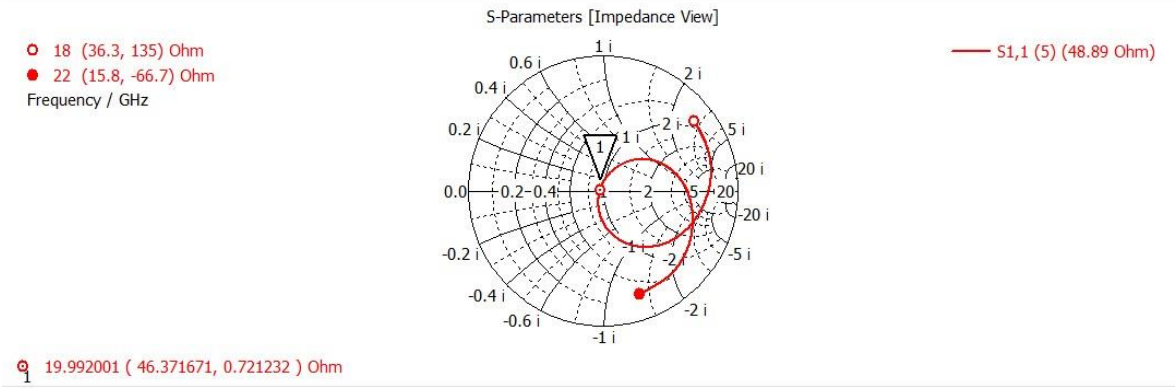

Figure 50: Smith Chart of the single-fed antenna.

The gain is presented in Figure 51 and Figure 52. The maximum value of the gain is 5.66dBi, in the direction of the z-axis. This shape shown in Figure 51 is the one expected for a patch antenna, with the maximum value of the gain above the patch, with the main lobe centered with the axis (Figure 52), and minimum below the antenna.

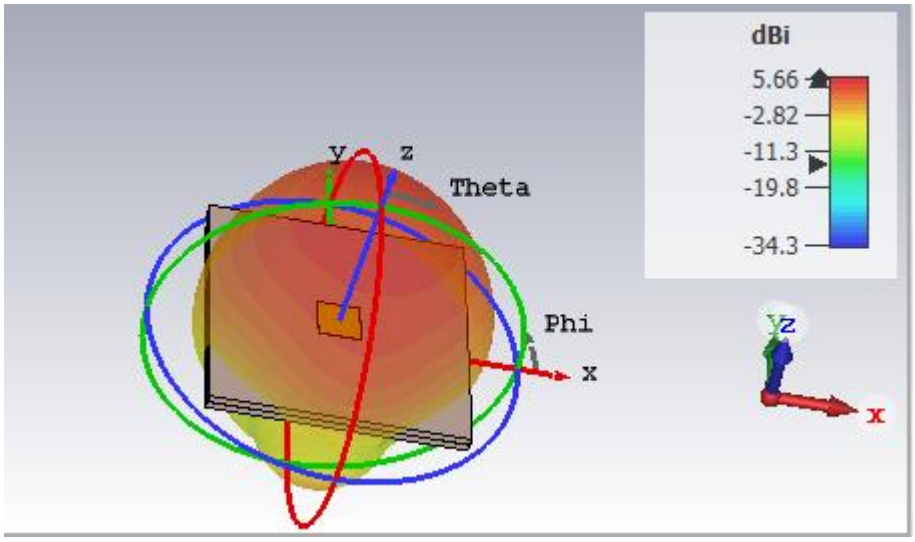

Figure 51: 3D radiation diagram of the single-fed antenna.

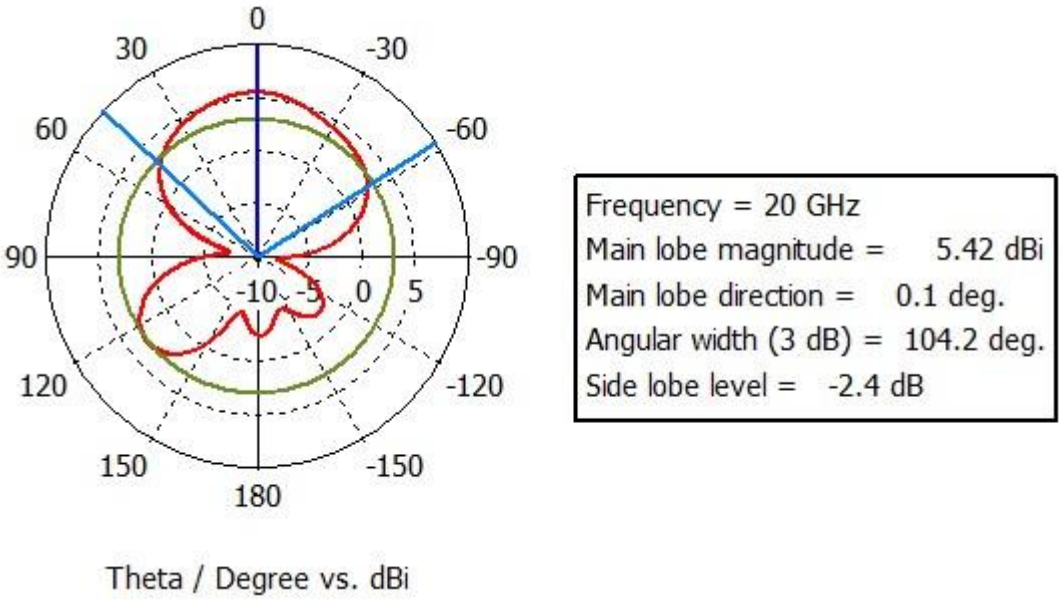

Figure 52: 1D radiation diagram of the single-fed antenna.

3.2 Design of the dual-fed patch antenna

After confirming that the results matched the requirements, the next step was the design of an antenna with dual feed. The dimensions were kept the same at first and then tuned as needed and are shown in Table 12.

Parameter	Value (mm)
Patch length (L)	3.41
Slot length (La)	1.6
Slot width (Wa)	0.25
H slot height (Lh)	0.57
Position of slot (Y1=-X2)	-1.35
Portion of line after slot center (Ls)	0.9
Width of 50Ω line (W0)	1

Table 12: Dimensions of the dual-fed patch antenna.

The feeding points are orthogonal and centered in the patch axes. At this point, the antenna became circularly polarized because of the orthogonal feeds.

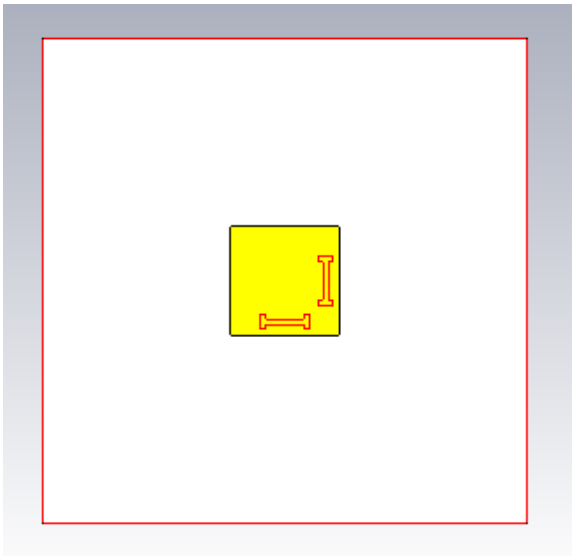

Figure 53: Top view of the dual-fed antenna.

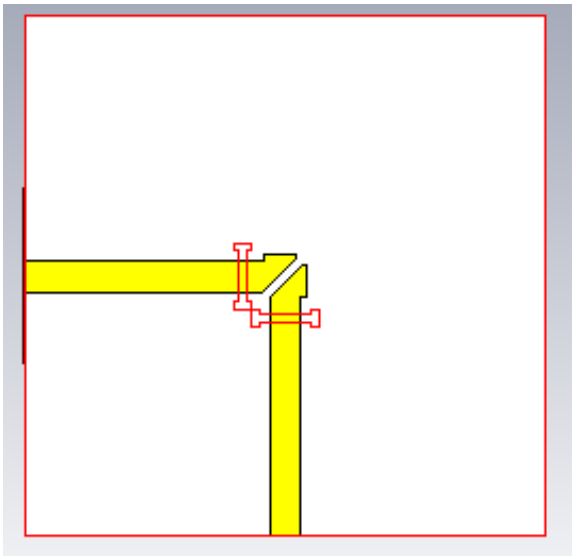

Figure 54: Bottom view of the dual-fed antenna.

Once again the dimensions had to be ajdusted until the results were acceptable. The transmission lines had to be bent and chamfered in order to have the correct length without overlapping. In this case, the ports must be simulated as simultaneous excitation, with a 90º phase shift.

Figure 55 and Figure 56 represent the results of the antenna's simulated S_{11}. The antenna is found to be well matched at the interest frequency, 20GHz, with an S_{11} of -

20.2dB. Additionally, a bandwidth of about 630MHz can be verified, which corresponds to 3% of the center frequency.

The S_{21} parameter (Figure 56) should also be taken into account here since it gives information on the interference between ports, ensuring the interference has a low enough value to not be a problem. The S_{21} at 20GHz is -9dB.

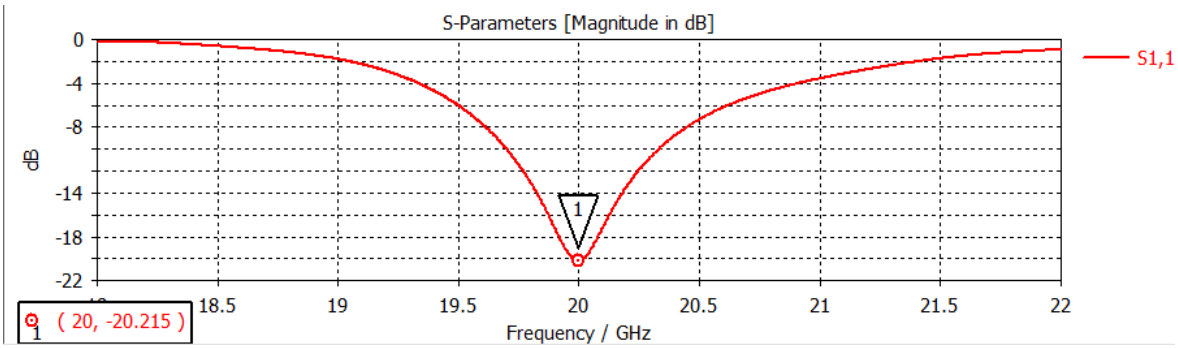

Figure 55: S_{11} of the dual-fed antenna.

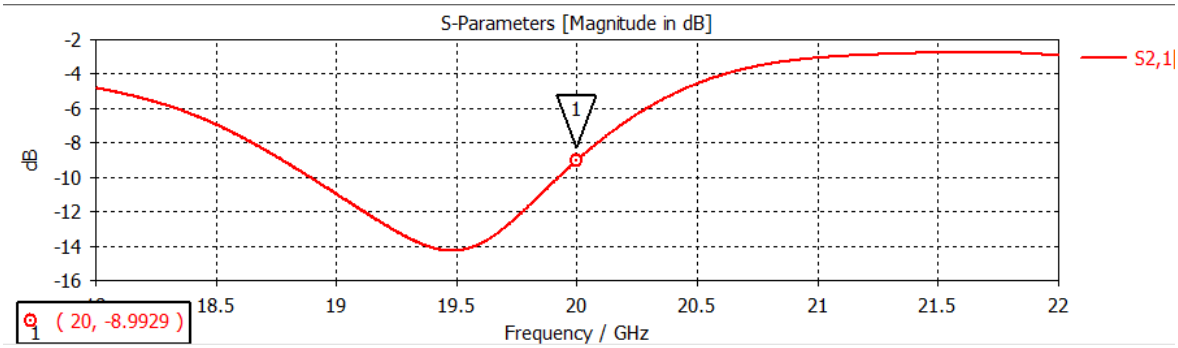

Figure 56: S_{21} of the dual-fed antenna.

The gain is presented in Figure 57 and Figure 58. The maximum value of the gain is 6.87dBi in the direction of the z-axis. In Figure 58 it can be noted that there is a slight shift of 2º in the direction of the main lobe.

Because of the dual feed, the antenna now presents circular polarization. This circular polarization is left because of the phase simulated in each port (0º in port 1 and 90º in port 2, the port at the bottom of Figure 54 and the other one, respectively) and could be inverted by interchanging these phases.

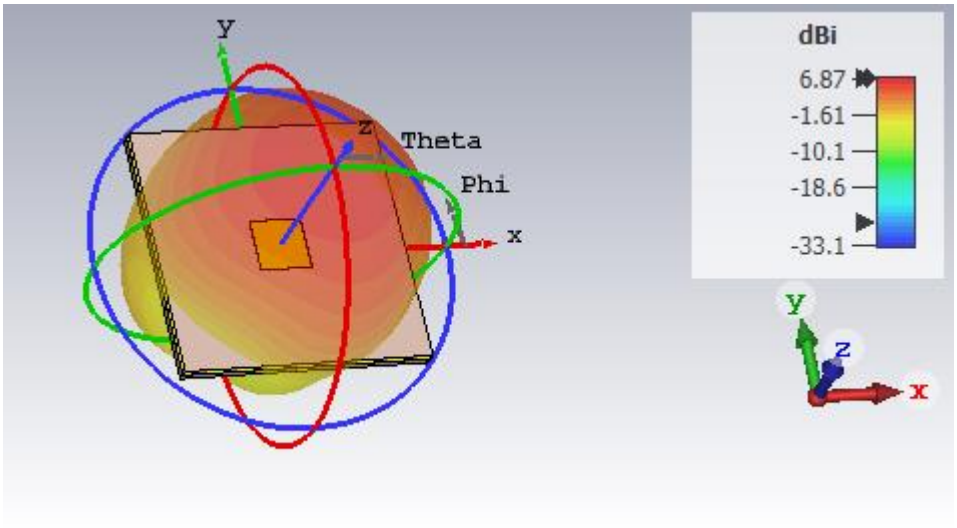

Figure 57: 3D radiation diagram of the dual-fed antenna.

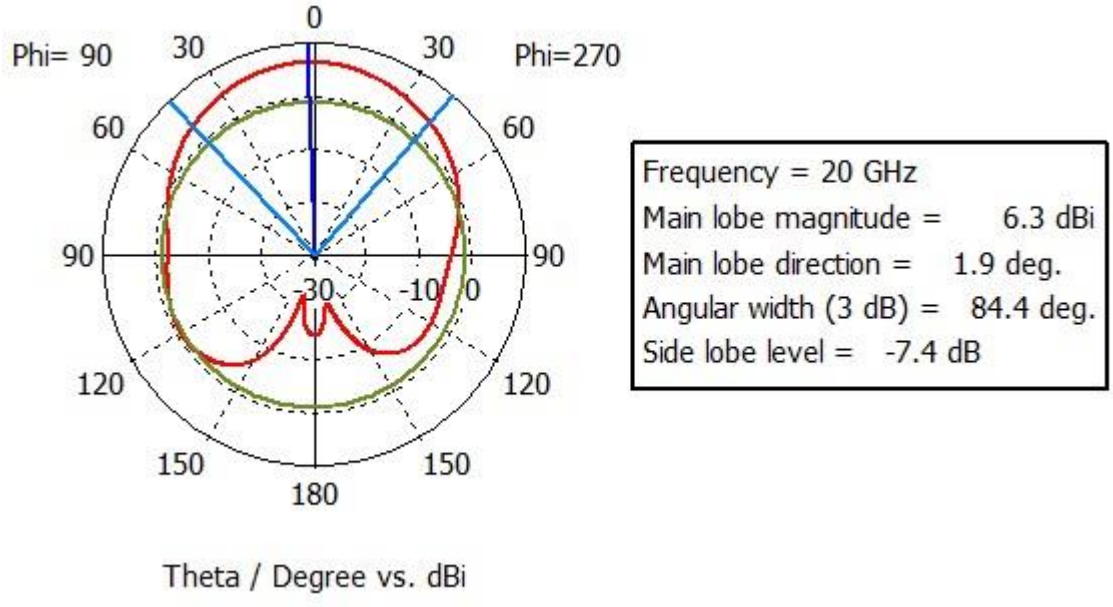

Figure 58: 1D radiation diagram of the dual-fed antenna.

It is important now to look at the Axial Ratio (Figure 59), to understand if the antenna is actually circularly polarized. For this to be true, the Axial Ratio needs to be smaller than 3dB at the operating frequency.

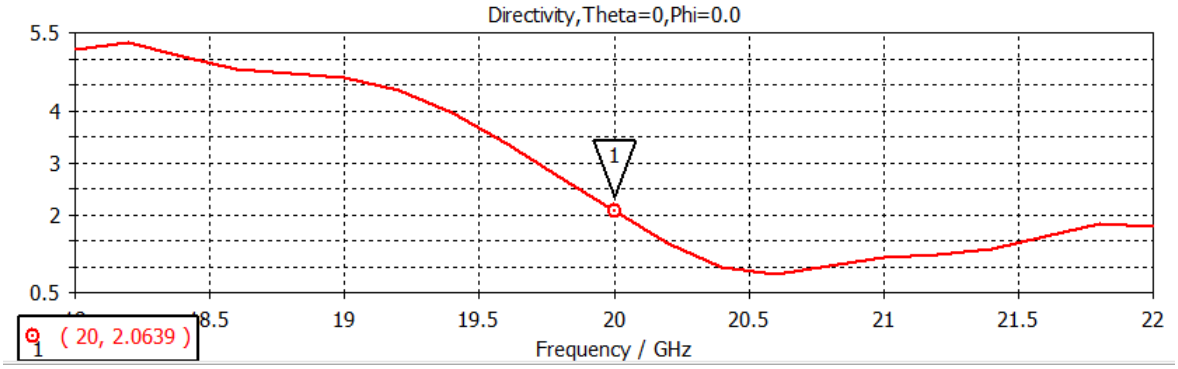

Figure 59: Axial ratio of the dual-fed antenna.

At this point we have a dual-fed antenna working at 20GHz, with minimum S_{11} at this frequency and acceptable S_{21} and with an axial ratio of 2dB (Figure 59), which means the polarization is circular. The maximum gain is also slightly higher than in the previous structure (Figure 51).

The next step in the designing procedure would be the insertion of a quadrature hybrid coupler for the feeding of the patch. Yet, this also had to be simulated to fine-tune the dimensions.

3.3 Design of the antenna fed by the hybrid coupler

The quadrature hybrid coupler is a device that splits the input signal into two output signals of equal amplitude (-3dB) and 90º apart in phase. To achieve this, its center segments should have a length of λ/4 and the horizontal thicker lines in Figure 60 have an impedance of $Z_0/\sqrt{2} = 35.4\Omega$ while the rest of the lines have impedance Z_0 = 50Ω.

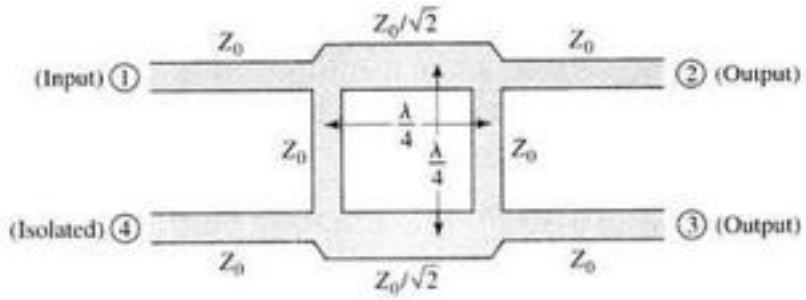

Figure 60: Quadrature Hybrid Coupler.

In order to achieve this, each line segment was measured (impedance and phase shift) with ports on either side and its dimensions tuned. These dimensions are shown in Table 13.

Parameter	Value (mm)
Length of 50Ω segments	2.2
Length 35Ω segments	2.25
Width of 50Ω segments	1
Width of 35Ω segments	1.1

Table 13: Dimensions of the hybrid.

The structure obtained is depicted in Figure 61.

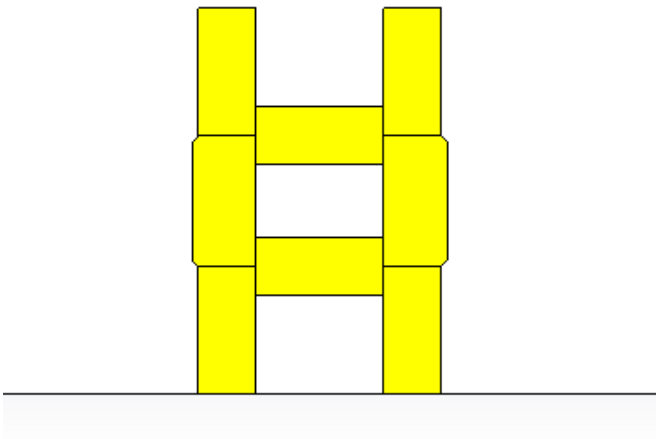

Figure 61: Quadrature Hybrid Coupler designed.

Simulating this structure with ports of the 4 ends, the analysis of the S_{11} (Figure 62) gives information about the losses that occur at the operating frequency; the S_{21} (Figure 63) describes the interference between the two input ports; the S31 and S41 quantify the losses (Figure 64) and phase shifts (Figure 65) between the input and the outputs.

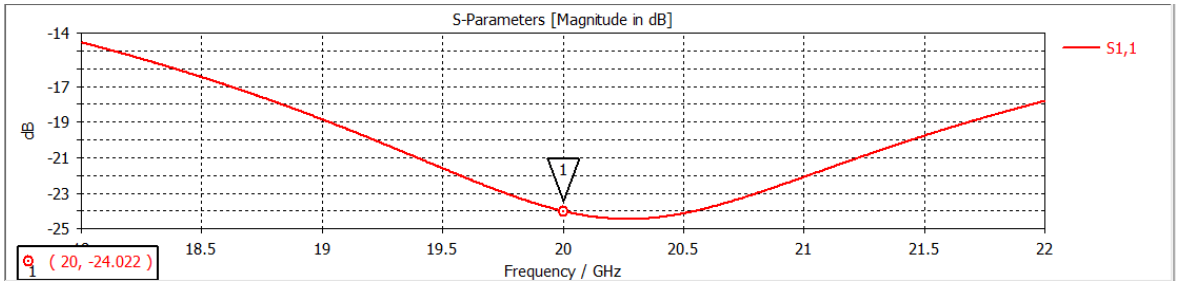

Figure 62: S_{11} of the hybrid coupler.

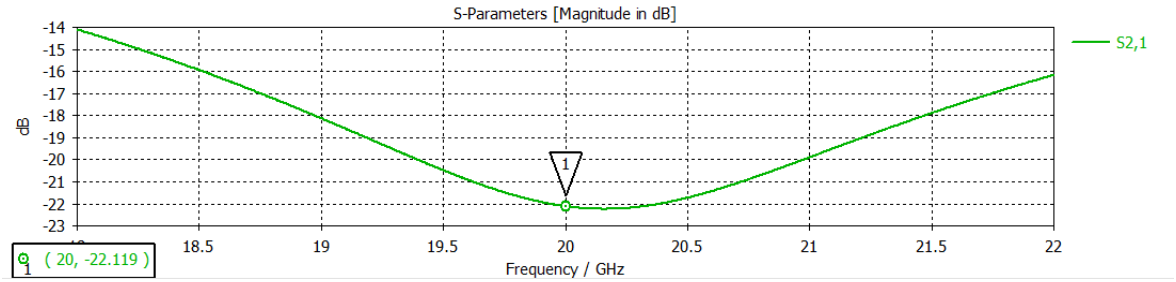

Figure 63: Interference between the two inputs of the hybrid.

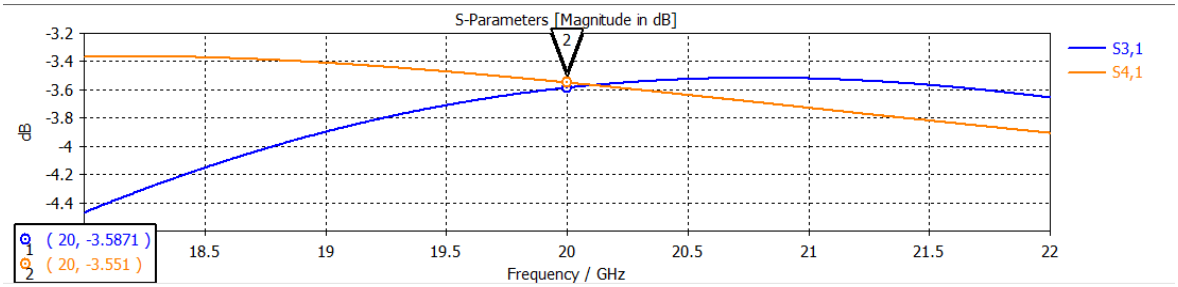

Figure 64: Magnitude in dB of the outputs of the hybrid.

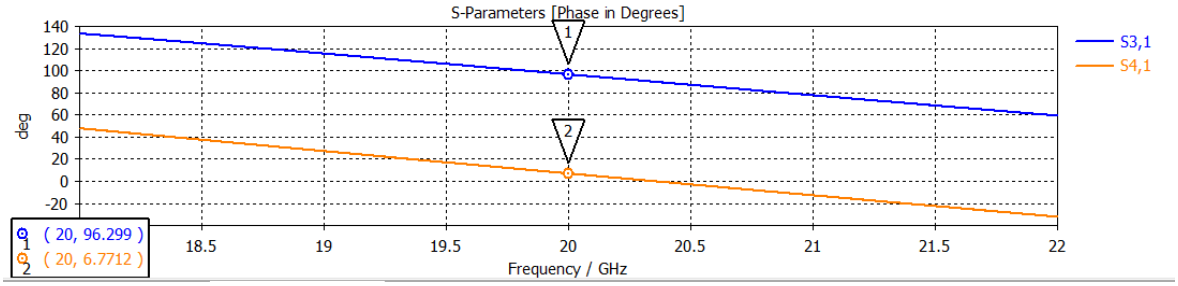

Figure 65: Phases of the outputs of the hybrid.

According to Figure 62, at the desired frequency, the quadrature hybrid coupler is well matched (S_{11} of -24dB), with the two inputs with low interference (-22dB, as shown in Figure 63), the magnitude of the outputs of about -3dB (Figure 64) and the phase difference of the outputs of 90º (Figure 65). This means it should function properly to the required effect.

Afterwards, both designs were integrated so as to use the hybrid to feed the dual-fed antenna, as shown in Figure 66 and Figure 67. By implementing the hybrid coupler to feed the antenna, this allowed for the orientation of the polarization (LHCP or RHCP) to be chosen by choosing which port of the coupler is fed by the input.

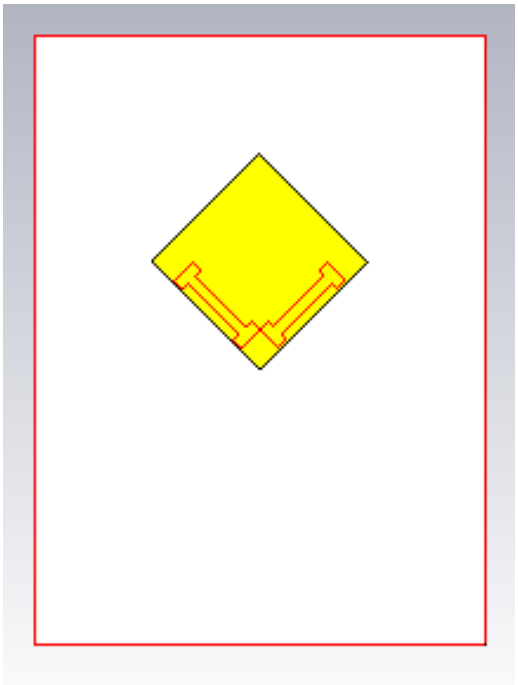

Figure 66: Top view of the dual-fed antenna with QHC.

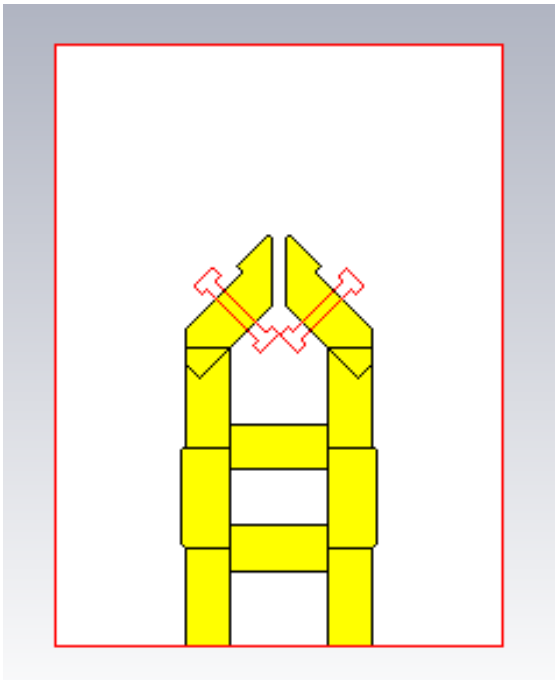

Figure 67: Bottom view of the dual-fed antenna with QHC.

This structure was then simulated, and small adjustments made to perfect the wanted operation.

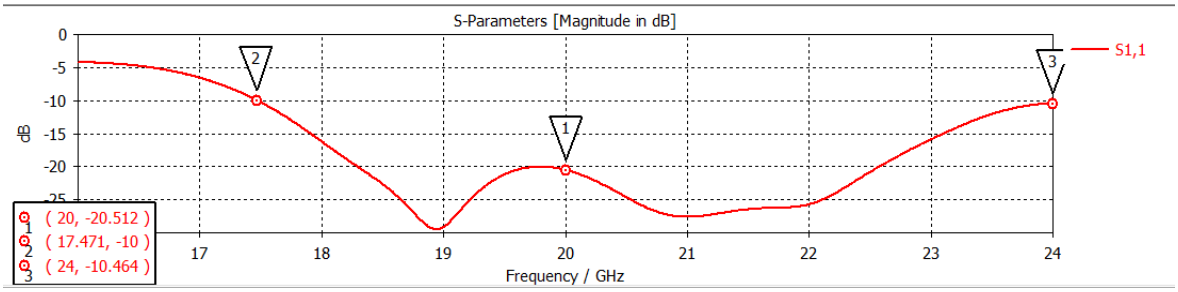

Figure 68: S_{11}/S_{22} of the antenna fed by the QHC.

The S_{11} of the antenna is equal to the S_{22} since it is symmetrical. As shown in Figure 68 this structure allows for a large bandwidth (about 6.6GHz, which is more than 30% of the center frequency) and has a S_{11} of -20.5dB at the operating frequency.

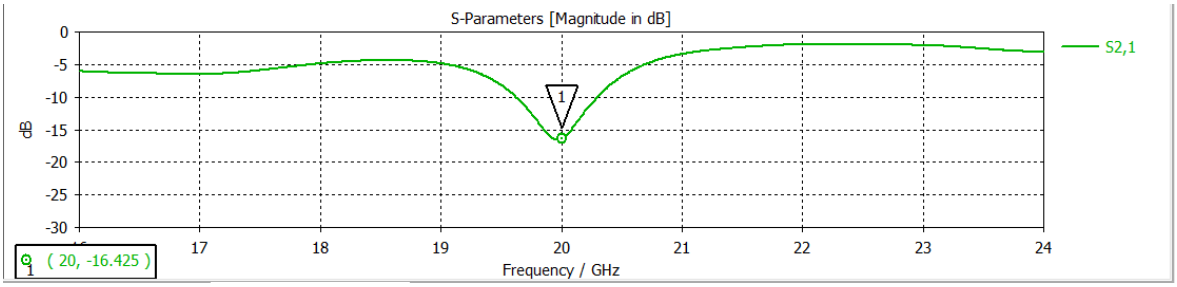

Figure 69: S_{21}/S_{12} of the antenna fed by the QHC.

The S_{21} is also the same as the S_{12} because, again, there is symmetry in the antenna. At the operating frequency, 20GHz, the S_{21} has a value of -16.4dB. This value is low enough to be satisfactory.

The gain and Axial Ratio of this antenna is shown in Figure 70 and Figure 71, respectively. The gain has a maximum value of 5.96dBi and the Axial Ratio is 2.1dB at 20GHz.

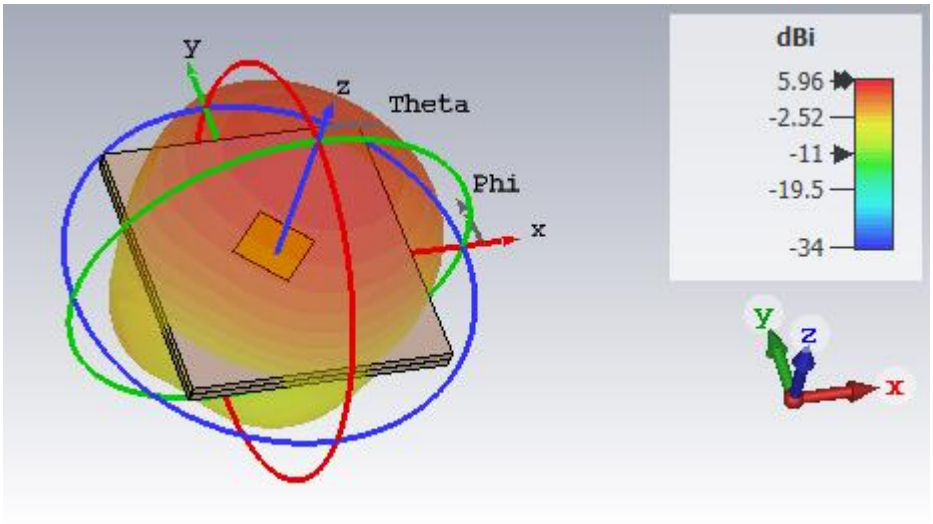

Figure 70: 3D radiation diagram of the antenna fed by the QHC.

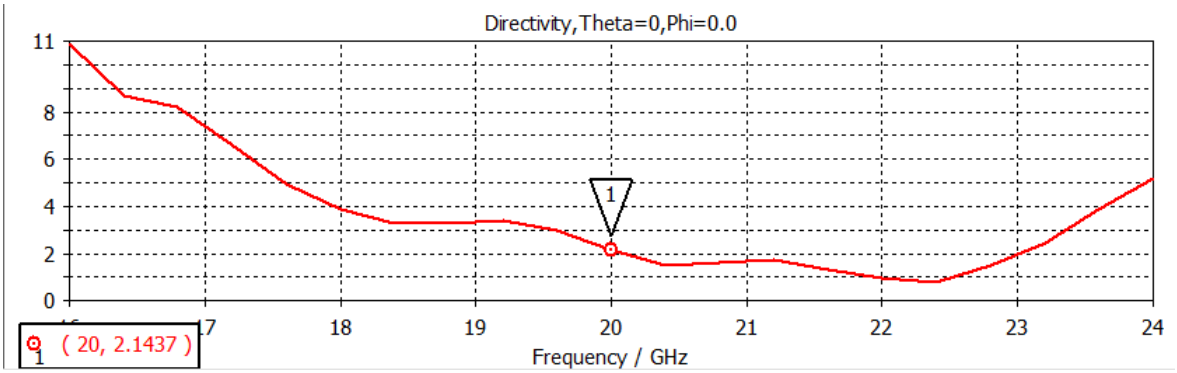

Figure 71: Axial ratio of the antenna fed by the QHC.

Thus, when the hybrid coupler is added to the structure the gain decreases slightly in relation to the one shown in Figure 57 and the axial ratio remains similar to the single fed antenna, which can be seen in Figure 59.

3.4 Design of the array

The next stage was the aggregation of 4 antennas into a 2x2 array with λ/2 distance between elements. Due to the hybrid coupler dimensions, it became clear that it was impossible to display the elements all in the same orientation, even after reducing the segments of the hybrid that don't affect the operation. For this reason, and taking into consideration the possible configurations of the feed lines of the array, a sequentially rotated configuration of the elements was selected (Figure 72 and Figure 73).

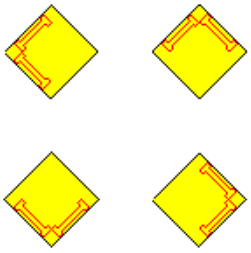

Figure 72: Top view of the array without feed lines.

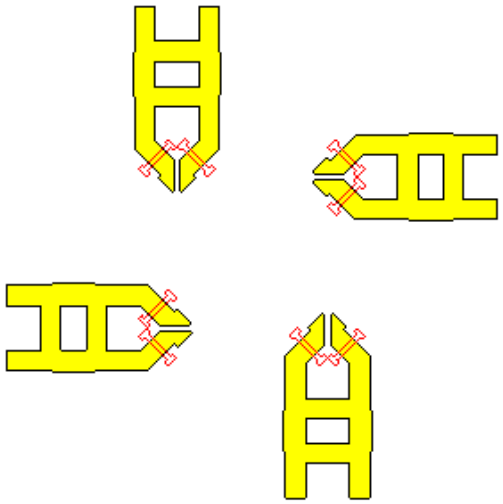

Figure 73: Bottom view of the array without feed lines.

Before starting the routing of the array feedlines, it is helpful to simulate the array with the ports directly at the inputs of the hybrid couplers. This simulation is done in the simultaneous mode, with the phase shifts required for the compensation of the rotation

of the array elements. The S11 parameter corresponding to both circular polarizations are shown below, in Figure 74 for the right polarization and Figure 75 for the left.

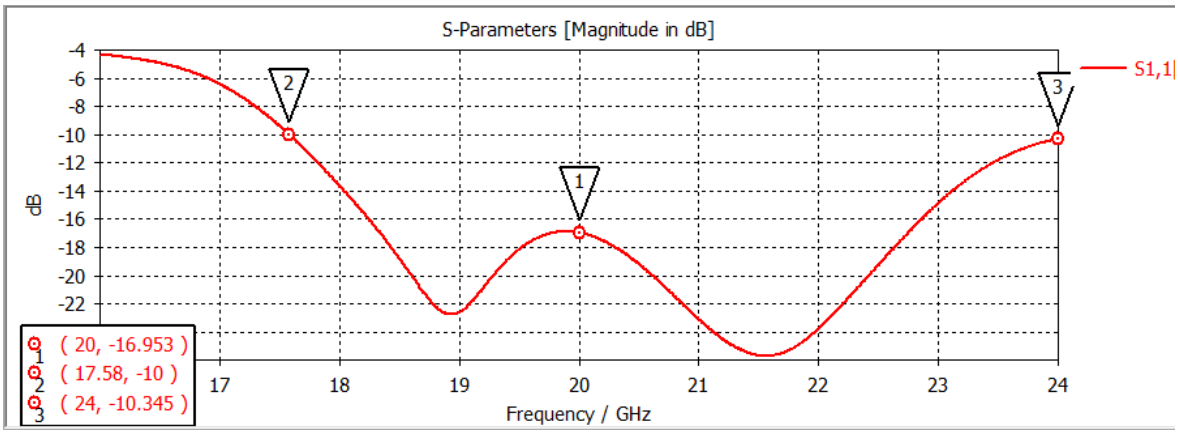

Figure 74: S_{11} of the array simulated without feedlines (in the RHCP mode).

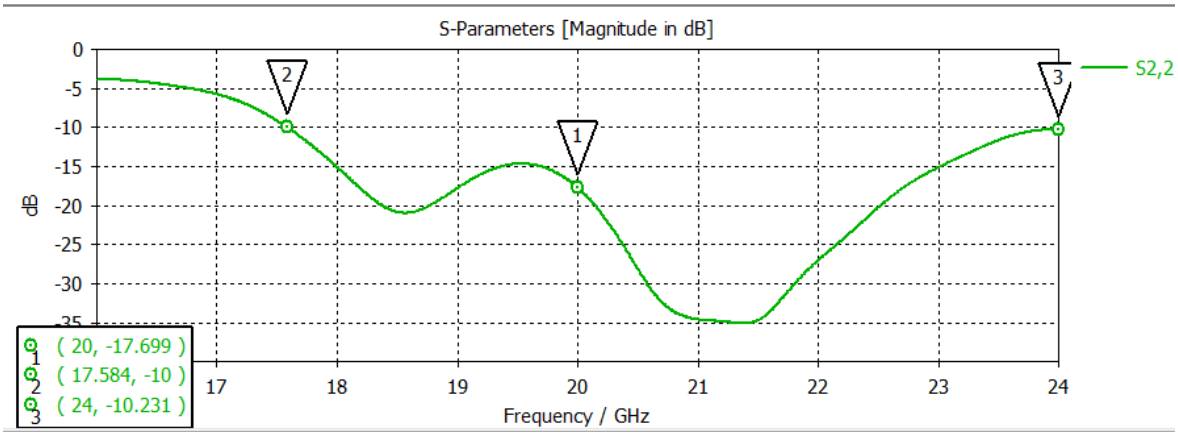

Figure 75: S_{11} of the array simulated without feedlines (in the LHCP mode).

The first graph, in Figure 74, shows the S_{11} of the right polarized configuration, which is -16.9dB at 20GHz and has a bandwidth of about 6.5GHz which corresponds to 32% of the operating frequency. The S_{11} of the left polarized antenna is -17.7dB at 20GHz and has a bandwidth of 6.4GHz, which is 32% of the center frequency.

The gain of the antenna in the RHCP configuration can be seen in Figure 76 and Figure 78 and the gain of the antenna in the LHCP configuration in Figure 77 and Figure 79.

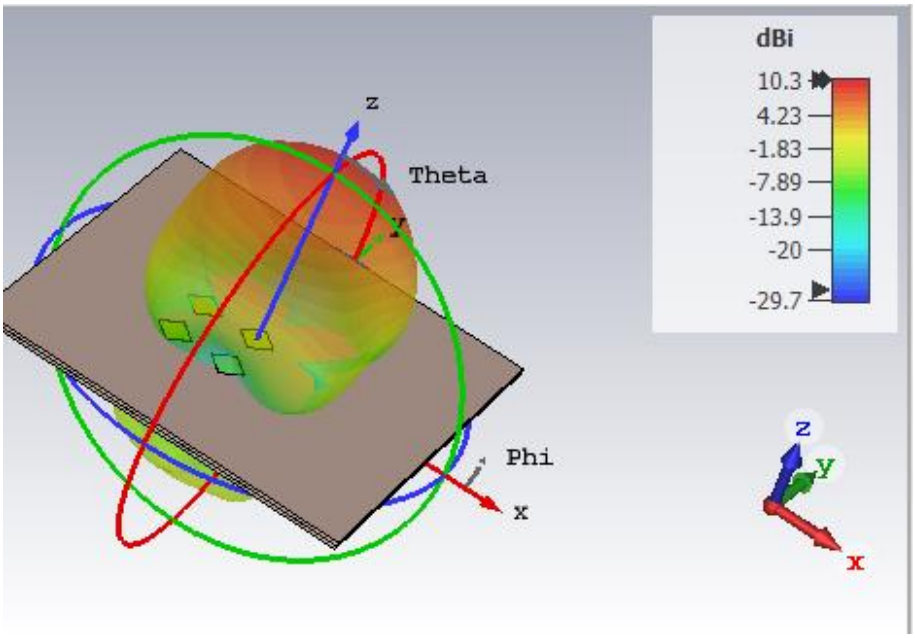

Figure 76: 3D radiation diagram of the RHCP array without feedlines.

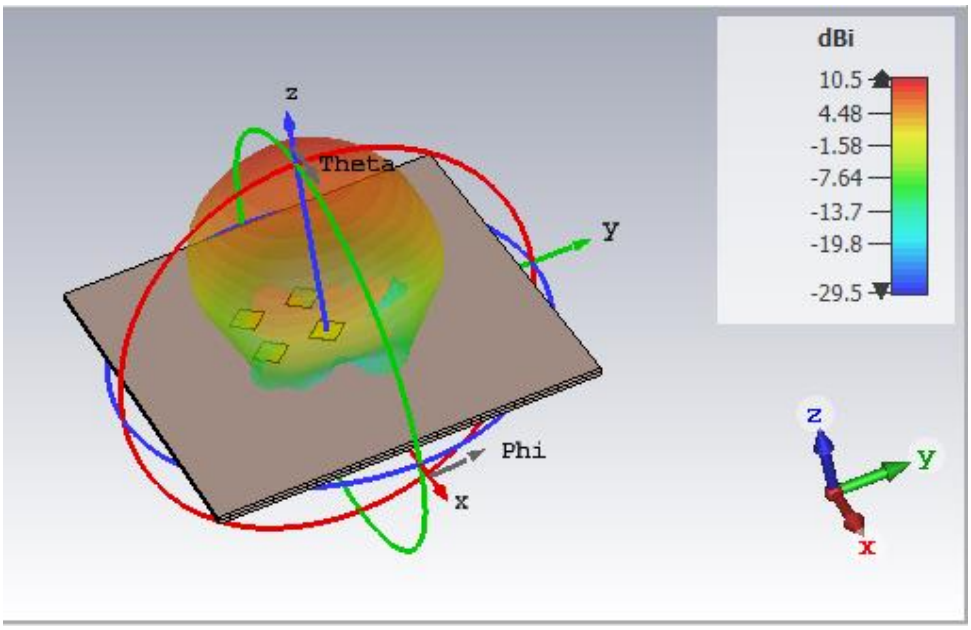

Figure 77: 3D radiation diagram of the LHCP array without feedlines.

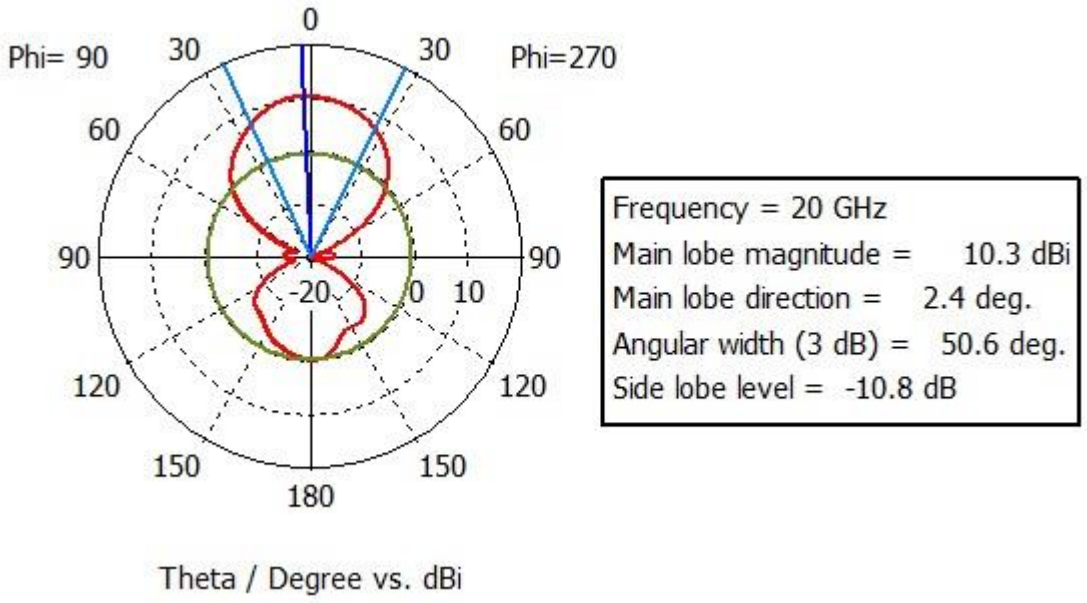

Figure 78: 1D radiation diagram of the RHCP array without feedlines.

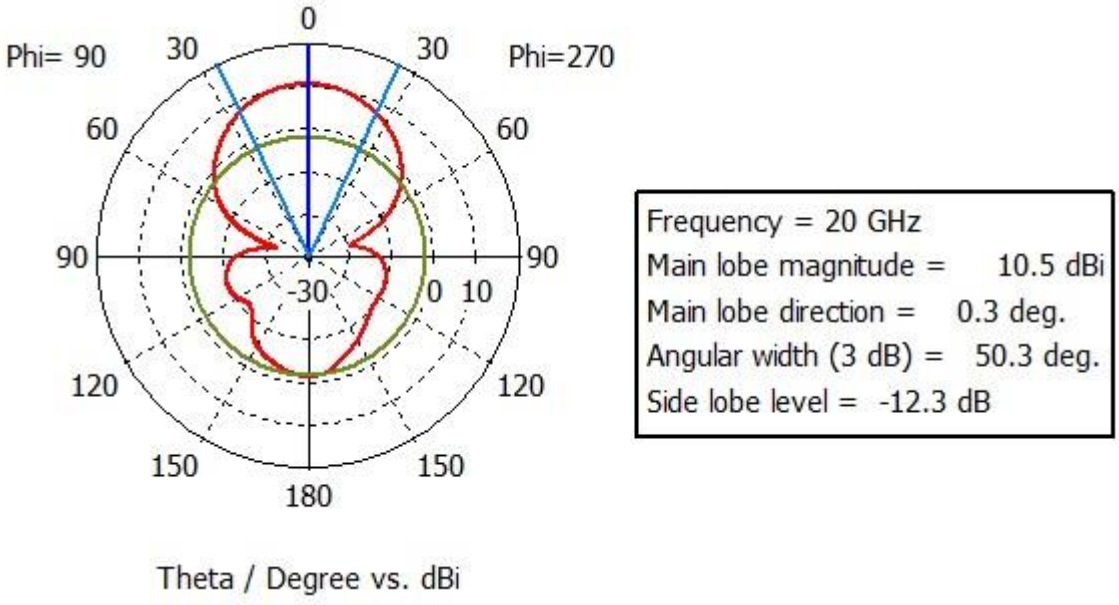

Figure 79: 1D radiation diagram of the LHCP array without feedlines.

For the RHCP configuration, the antenna has a maximum value of gain of 10.3dBi and the direction of the main lobe is shifted by 2º. For the LHCP configuration, the antenna has a maximum gain of 10.5dB and no shift in the main lobe direction.

Even though the array should remain symmetrical, the results are different for one polarization and the other (RHCP and LHCP). In spite of this, the results are still good, and the gain has increased from the individual elements. However, the back lobe is also starting to increase, even before the addition of the feed lines for the array.

In Figure 80 and Figure 81 are presented the Axial Ratio graphs as a function of frequency. Our goal for the prototype is that the Axial Ratio is kept below 3dB for a large bandwidth around the operation frequency (20GHz).

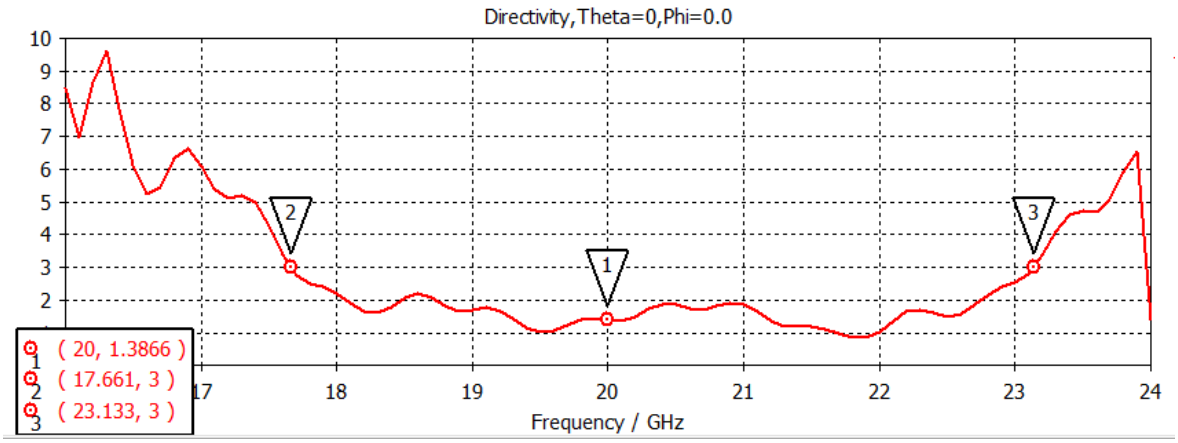

Figure 80: Axial ratio for the RHCP.

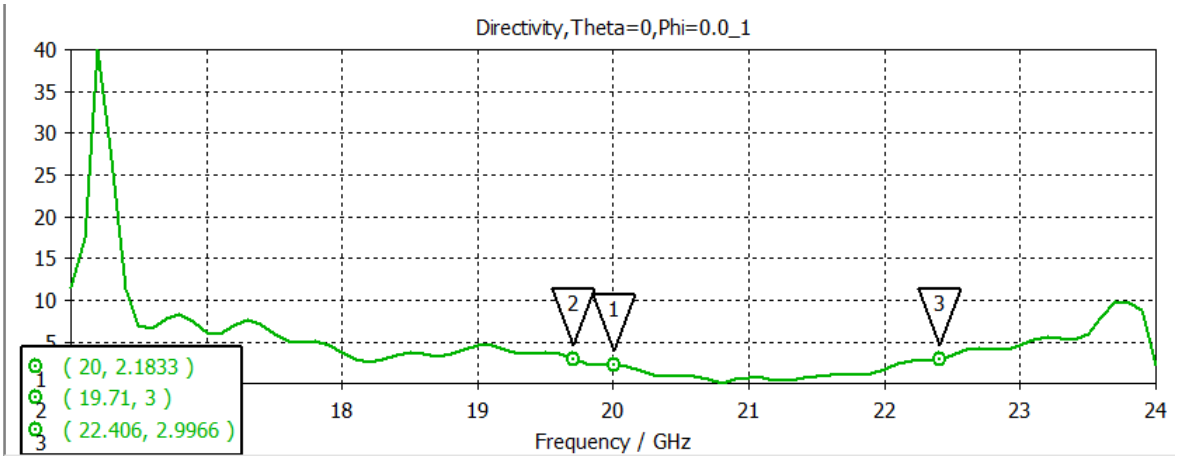

Figure 81: Axial ratio for the LHCP.

The RHCP (Figure 80) maintains a large band (more than 5GHz) of circular polarization, however the LHCP (Figure 81) has degraded a bit, having circular polarization in a band of almost 3GHz.

The routing of the feedlines without overlapping the lines of both the polarizations proved to be the biggest challenge. The rotation of the antenna elements needed to be compensated by tuning the phase shift of the array feeding lines. The RHCP, which corresponds to the right inputs of the hybrid couplers (in the perspective of Figure 73), requires the elements to have sequentially a phase shift of -90º (for example 0º, -90º, 180º, 90º). On the other hand, the LHCP, which corresponds to the left inputs of the

hybrid couplers, requires the elements to have a phase shift of 90º (for example 0º, 90º, 180º, -90º).

The use of 50Ω lines would take up too much space and increase the interference between lines so the use of thinner lines was preferred. For the transformation to 100Ω lines, quarter-wavelength transformers were used. To design a quarter-wavelength transformer, a line of λ/4 length must be used, with proper width to achieve an impedance of

$$Z_1 = \sqrt{Z_L Z_{in}}$$

Where Z_{in} is the impedance at the input of the transformer and Z_L the impedance at the output. Thus, $Z_1 = 70.7\Omega$, W1 = 0.6 mm and L70 = 2.3 mm.

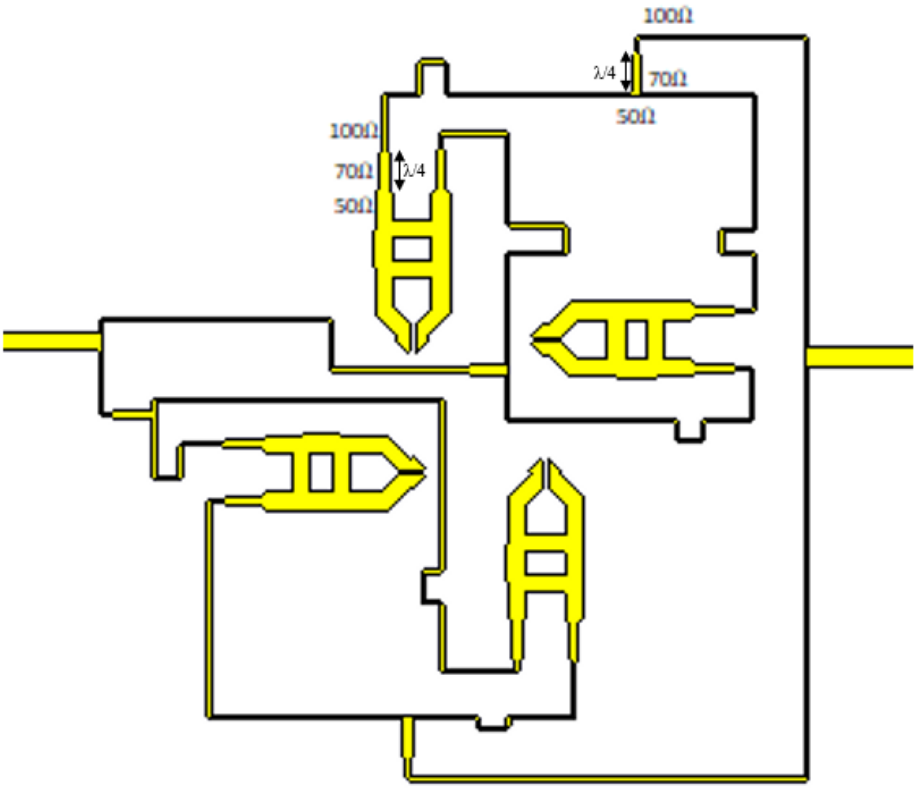

Figure 82: Feeding Lines of the array.

When two 100Ω lines join, the joined impedance because they are in parallel is again 50Ω. At those points, the quarter-wavelength transformers calculated previously are again used to obtain 100Ω lines, which are easier to use. When all the lines meet in the end, a 50Ω line segment is placed to connect to a port. The U-shaped indentations seen in Figure 82 have the purpose of facilitating the tuning of the phase shift imposed by the

line lengths. By increasing the height of these indentations, the phase-shift imposed by the line will also increase, until the needed values are achieved. All the corners of the lines were chamfered in an attempt to improve the efficiency of this feed network.

The results of the simulation of this prototype will be presented and discussed in the next chapter to ease the comparison with the measurements.

After the designing of the antenna prototype, the structure had to be prepared for fabrication and so some holes for the connectors and Teflon screws had to be added. The resulting design is shown in Figure 83 and Figure 84.

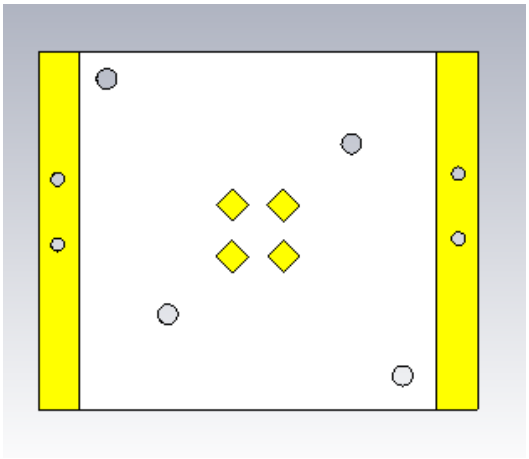

Figure 83: Prototype to fabricate (top view).

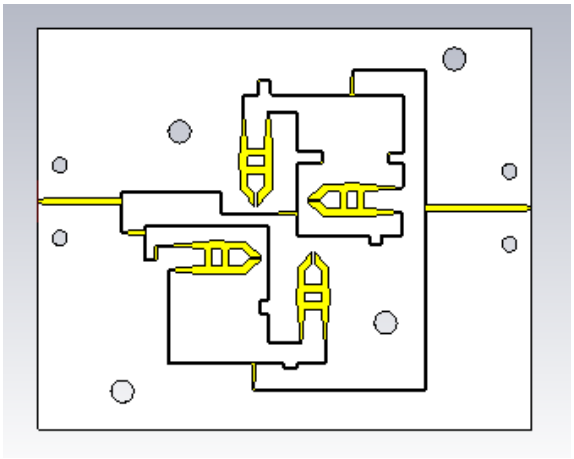

Figure 84: Prototype to fabricate (bottom view).

Lastly, a study of the behavior of the array with the implementation of copper vias around the patches was done. The purpose of this experiment was to try to reduce the mutual coupling in the array and improve the radiation efficiency [26].

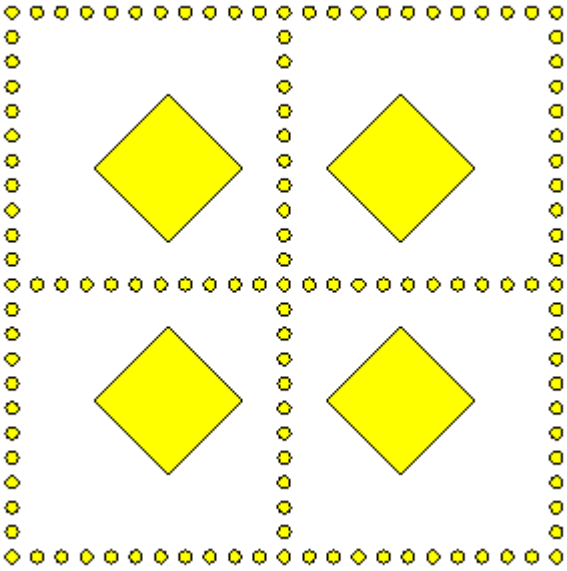

Figure 85: Array with vias around the patches.

This study was done by taking the structure depicted in Figure 72 and Figure 73 and simulating it with and without the addition of the vias around the patches. These copper vias in Figure 85 connect the top of the substrate with the ground plane, with the purpose of suppressing surface waves, improving radiation efficiency and reducing coupling [26].

Ports were added to each input of the quadrature hybrid couplers (see Figure 73). Then by comparing two analogous inputs of adjacent patches, the interference between ports was compared in the two cases (with and without vias).

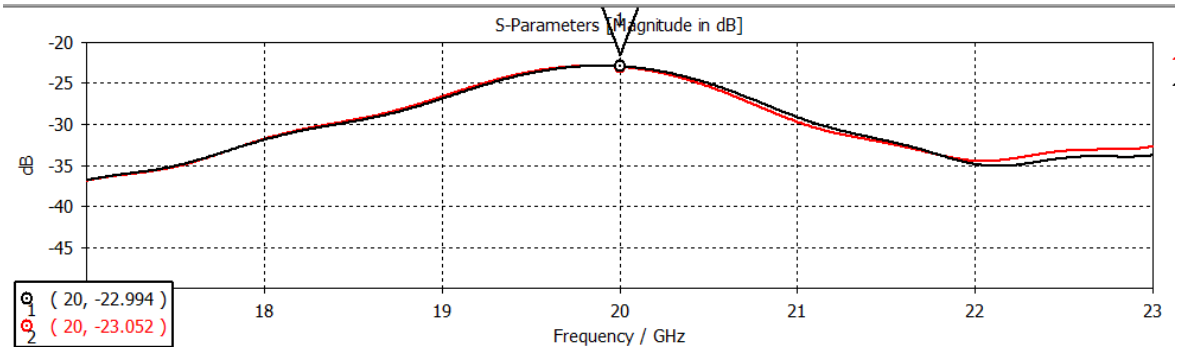

Figure 86: Comparison of the S1,3 with vias (red) and without vias (black).

Taking for example ports 1 and 3 (which correspond to two right arm inputs of the hybrids feeding adjacent patches), the result of the comparison is shown in Figure 86.

Taking then non-adjacent patches (patches diagonal to one-another), but still analogous ports, the results of the coupling of port 1 and port 5 are shown in Figure 87.

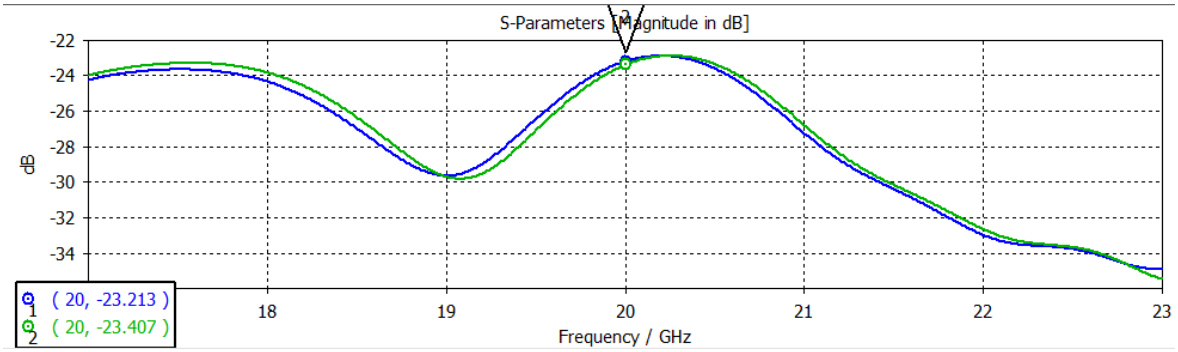

Figure 87: Comparison of the S1,5 with vias (green) and without vias (blue).

While it can be noted that in both cases the values are lower for the structure with vias, it is not significant enough to proceed with the addition of this technique to the prototype.

4 Implementation and results

4.1 Simulation results

The structure with the feeding lines depicted in Figure 82 was simulated and is shown below in Figure 88 and Figure 89.

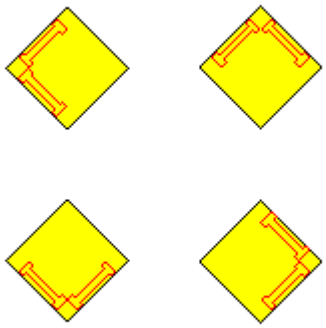

Figure 88: Antenna array top view, with the ground slots delineated in red.

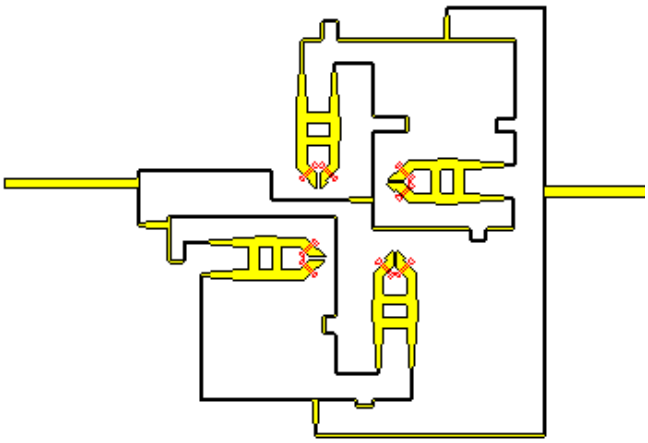

Figure 89: Antenna array bottom view, with the ground slots delineated in red.

This antenna array is the sequential evolution of the structures so far presented. Each individual element has been designed and simulated in the previous chapter and then aggregated into a 2x2 array, with sequentially rotated elements. After the routing of the array feed lines, this array presented the following results:

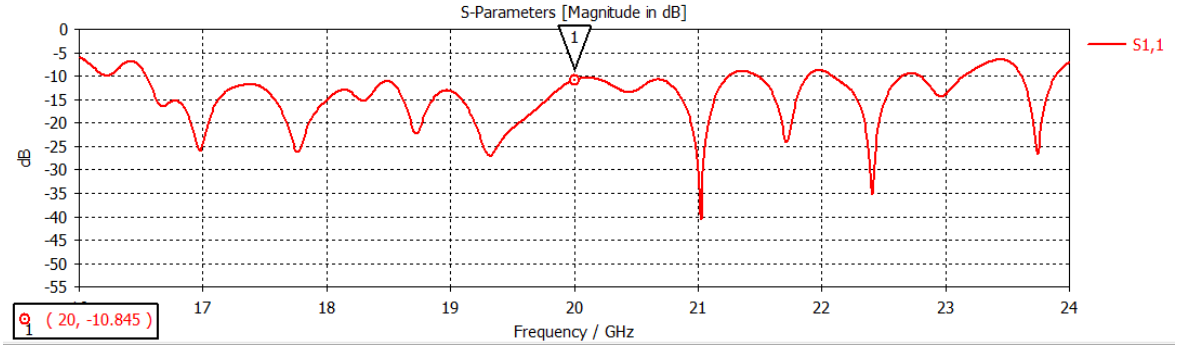

Figure 90: S_{11} of the antenna array, In the RHCP mode.

In comparison with the previous stage, in Figure 74, one can already state that the addition of the array feeding lines has greatly degraded the performance of the antenna prototype. While, before, the band had well defined boundaries (always well below the

−10dB limit inside the band), and had good performance all throughout the band, in this version the S_{11} is very irregular, and many times comes close (or even above) the -10 dB limit.

It is fundamental to also analyze the gain and axial ratio to understand if the rest of the requirements can be met with this antenna array.

In Figure 91 and Figure 92, the gain for the RHCP configuration of the antenna is shown.

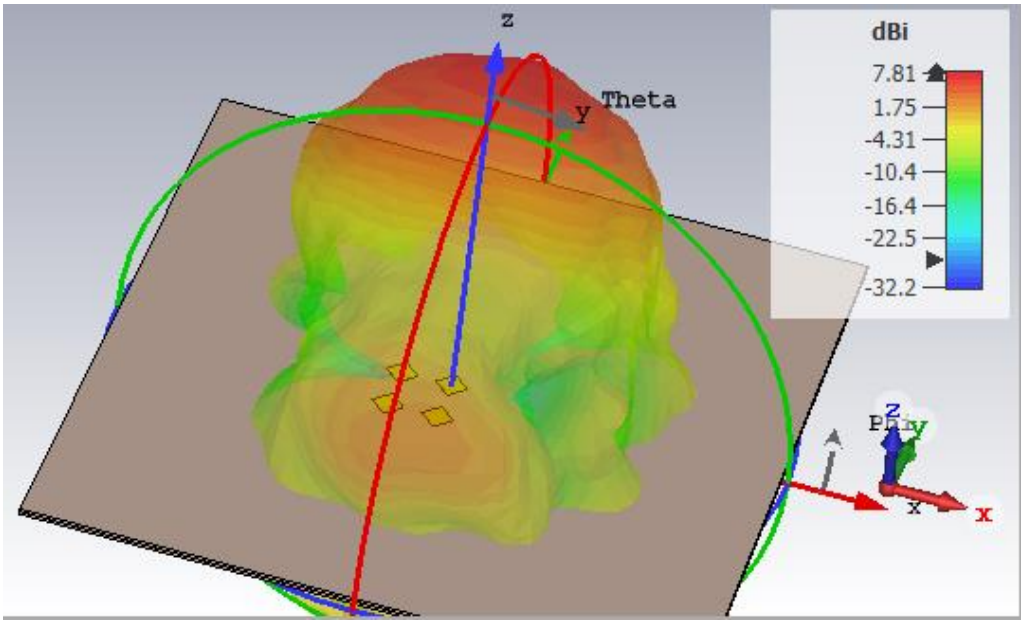

Figure 91: Radiation diagram for the RHCP mode.

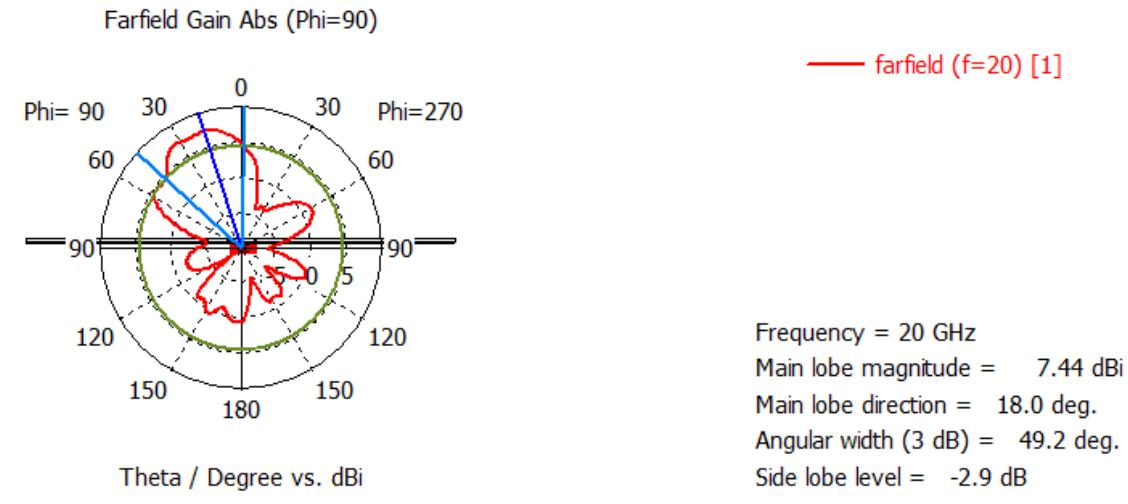

Figure 92: 1D representation of the gain of the RHCP mode.

The radiation diagram has also worsened. The magnitude of the main lobe decreased almost 3 dB (from 10.3dB in Figure 76 to 7.4dB) and has deviated 18º from the center. The back and side lobes have remained at an acceptably low level.

Afterwards, the other port was simulated in order to see the results for the left polarization (LHCP). While the two should be symmetrical (which would make the results similar for both polarizations), it is expectable that they should diverge since the lines feeding the array are completely different for each port.

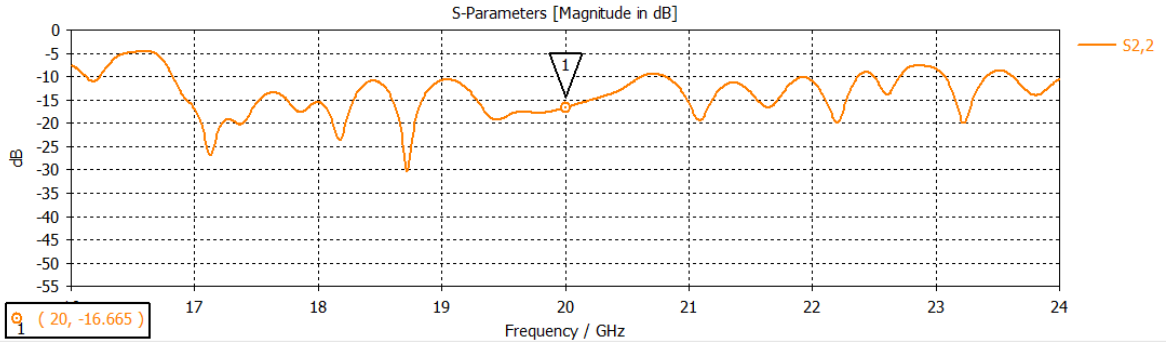

Figure 93: S_{11} of the antenna array, In the LHCP mode.

Once again, when comparing Figure 93 with Figure 75, the S_{11} of the antenna operating in the left polarization mode has a very reduced bandwidth. Because -10 dB is the limit used to measure bandwidth, and the graph in Figure 93 is very irregular, getting several times close and above this limit, the bandwidth of more than 6GHz achieved in the previous stage (Figure 74) has severely diminished.

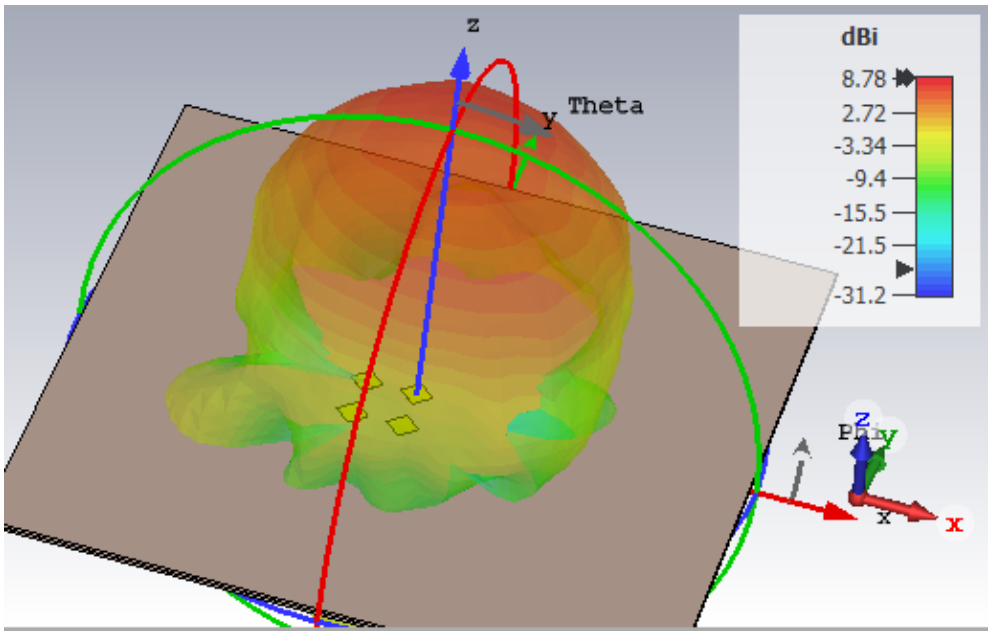

Figure 94: Radiation diagram for the LHCP mode.

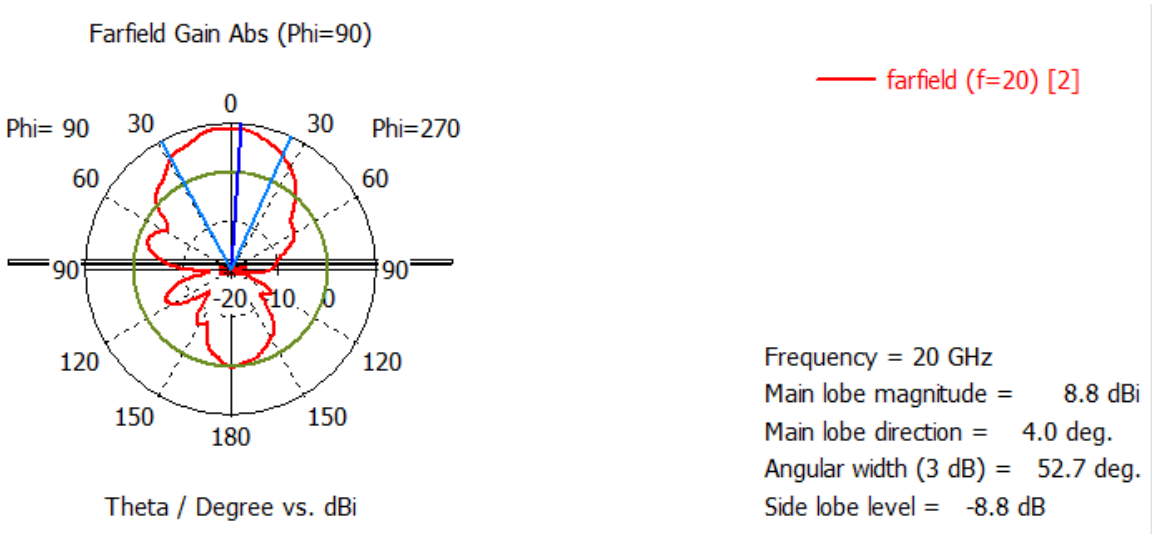

Figure 95: 1D representation of the gain of the LHCP mode.

The main lobe has decreased from 10.5dB in the previous stage of Figure 77 and Figure 79, assumed a more irregular shape and has a 4º deviation from the center. This should also impact the axial ratio of the antenna. The back lobe has also changed shape but hasn't changed much in terms of magnitude.

Now looking at the S_{21} in Figure 96, one can verify that the ports don't have much correlation with one another in the operating frequency band, assuming a value of −20dB.

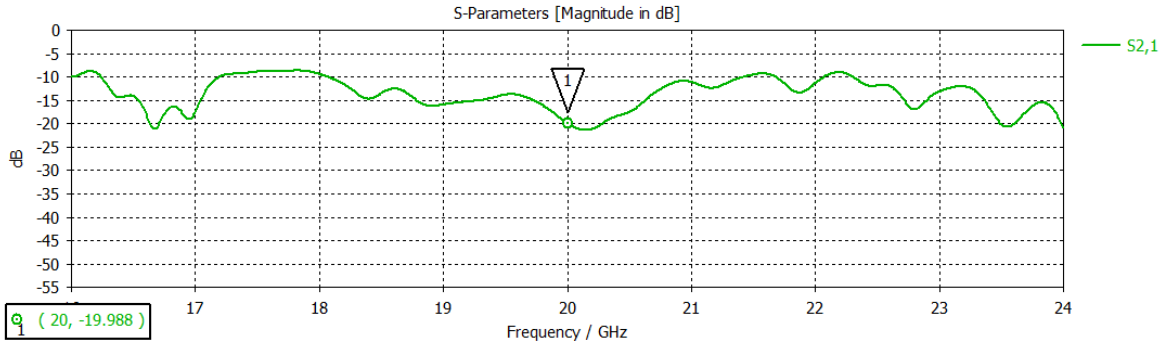

Figure 96: Correlation between both ports of the antenna.

Finally, it is important to analyze the Axial Ratio of both configurations (RHCP in Figure 97 and LHCP in Figure 98) to confirm that the circular polarization is ensured.

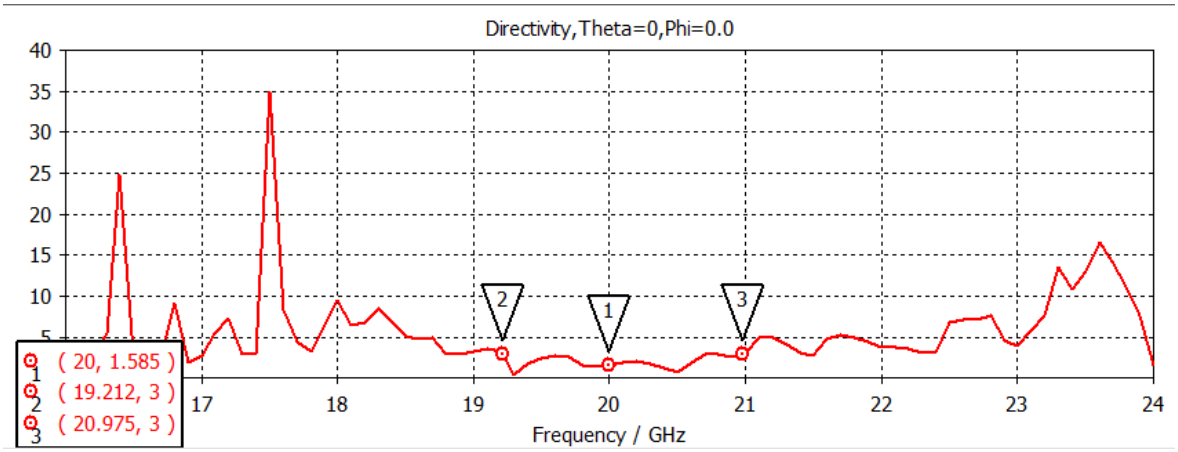

Figure 97: Axial ratio of the RHCP configuration.

The axial ratio corresponding to the RHCP configuration has a very irregular pattern. At the center frequency it has a value of 1.58dB which means the polarization is circular. However, where there was a band of circular polarization of more than 5GHz before (Figure 80), now there is a bandwidth of less than 2GHz.

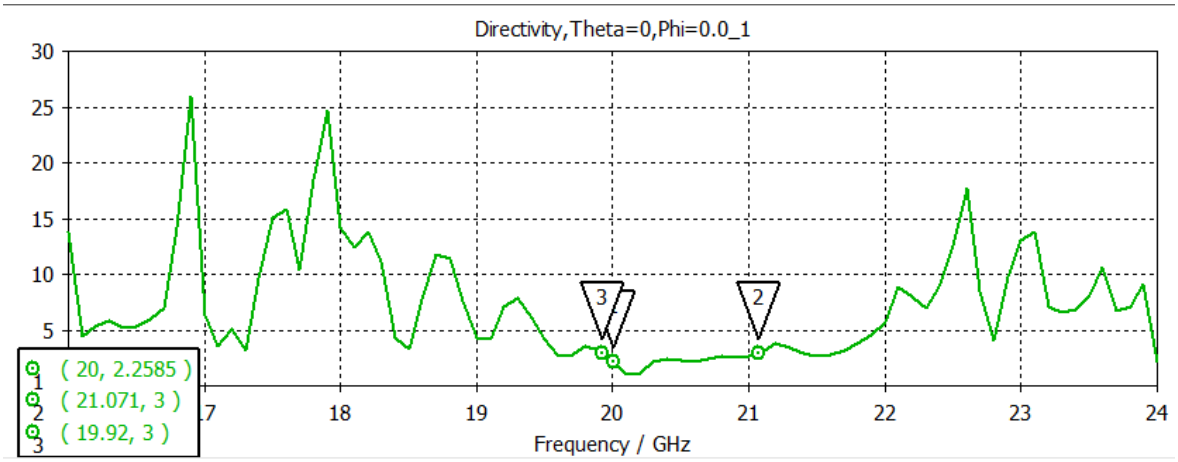

Figure 98: Axial ratio of the LHCP configuration.

For the left polarization, another very irregular pattern takes place in the axial ratio graph as a function of frequency. At the center frequency the circular polarization is ensured, with a value of 2.26dB (< 3dB), but the bandwidth in which the antenna radiates circularly has been reduced from almost 3GHz in Figure 81 to about 1GHz in Figure 98.

The initial specifications of the project stated that the antenna designed should have a wide bandwidth and a circular polarization in this bandwidth. Even though the results obtained in the simulations don't perfectly fit the requirements, the prototype continued for fabrication.

4.2 Measurements

The prototype antenna of Figure 83 and Figure 84 was constructed and is shown in Figure 99 and Figure 100. Due to the limitations of the manufacturing tools available, the production of the antenna was made in two separate modules. One of them with the patches and top substrate and the other with the ground plane, bottom substrate and feeding network. These two parts were united with Teflon screws, which fit into the holes already included in the design of Figure 83. The SMA connectors, model 292-04A-6, were also attached to the ends of the board, connecting to the transmission lines that feed the array. These lines had to be tapered so that they would fit the connector's maximum width (Figure 84).

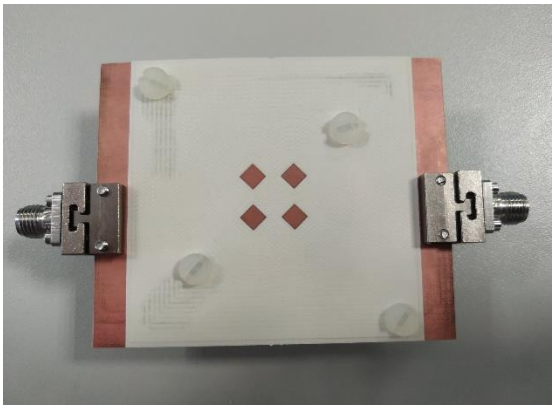

Figure 99: Top view of the produced prototype.

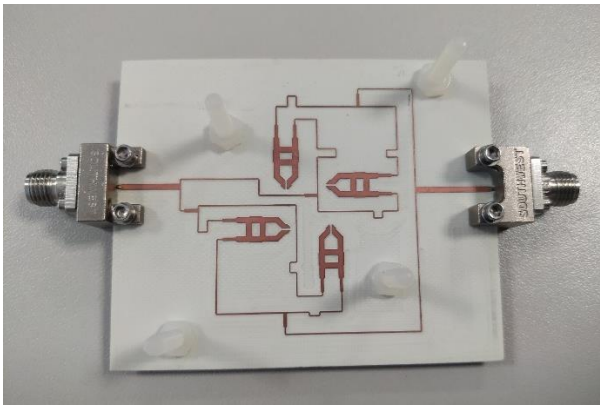

Figure 100: Bottom view of the produced prototype.

The first step in the measurements of the antenna's parameters was the measurement of its S_{11} parameters for both polarization configurations. For this purpose, a VNA (Vector Network Analyzer) was used, after calibration of the equipment. The results obtained were superimposed with the simulation results for these parameters and are shown below.

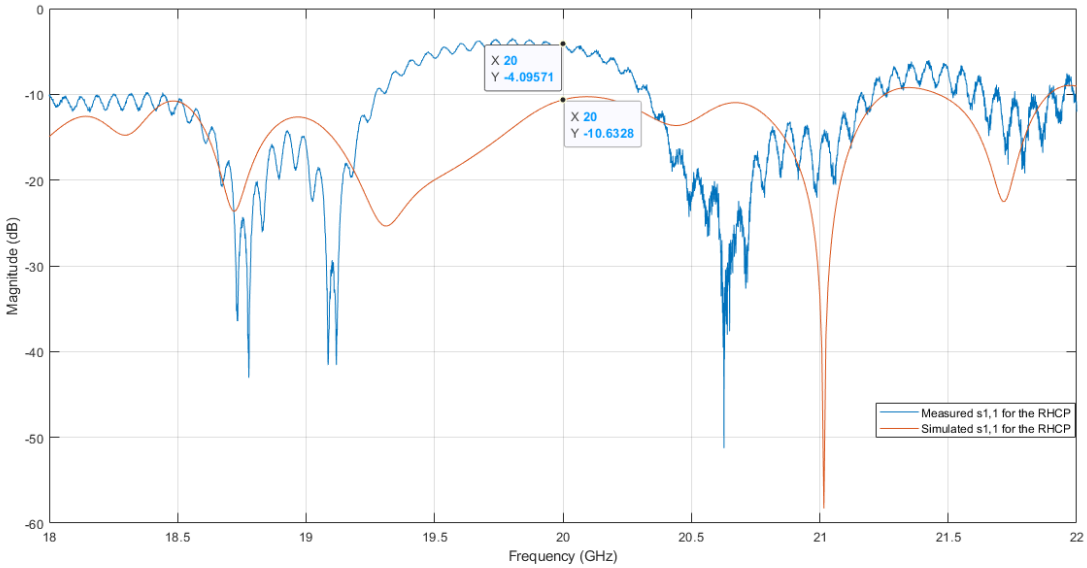

Figure 101: Comparison of the simulated and measured S_{11} of the RHCP antenna.

The first port to be measured was the one that imposes right polarization. A 50Ω load was connected to the remaining port to ensure it was matched. The result of this measurement can be observed in Figure 101, where the blue line is the measured S_{11}, and the red line is the simulated.

After, the same was done for the other port, and the results registered (Figure 102).

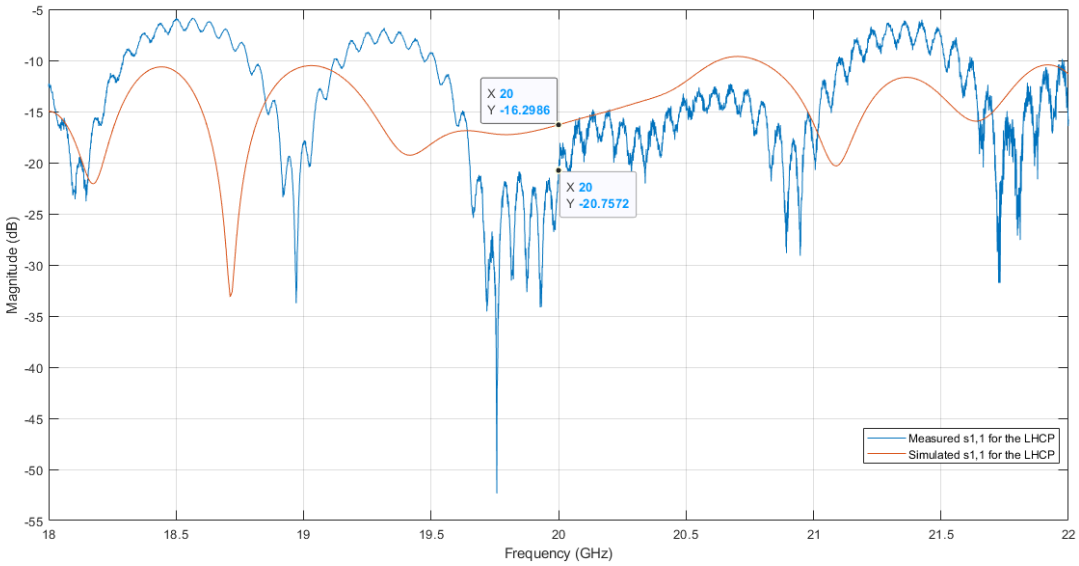

Figure 102: Comparison of the simulated and measured S_{11} of the LHCP antenna.

The next step in the procedure was the assembly of a setup (Figure 103 and Figure 104) to allow measurements to be made in the anechoic chamber. The prototype antenna was attached to a tripod and aligned with an emitting antenna, with the aim of measuring the reception with the prototype. For each polarization, the S_{21} was measured in the vertical position and then the transmitting antenna, which is linearly polarized, was rotated to measure the orthogonal position. When this rotation was done, the antennas had to be realigned. It was done this way for simplicity since the rotation could have been made in the receiving antenna.

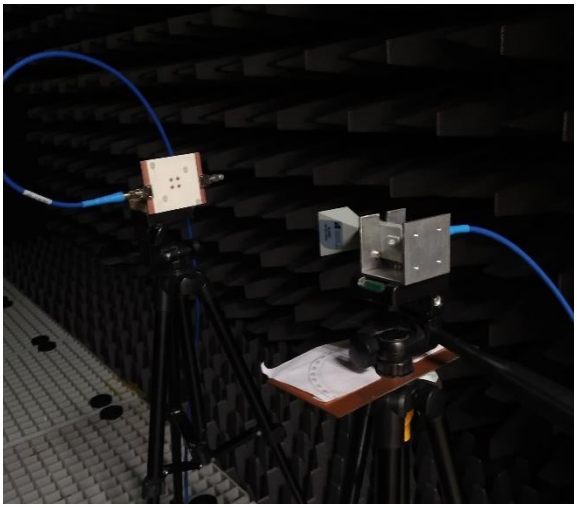

Figure 103: Photograph of the setup in the anechoic chamber, with the transmitting antenna in the vertical position.

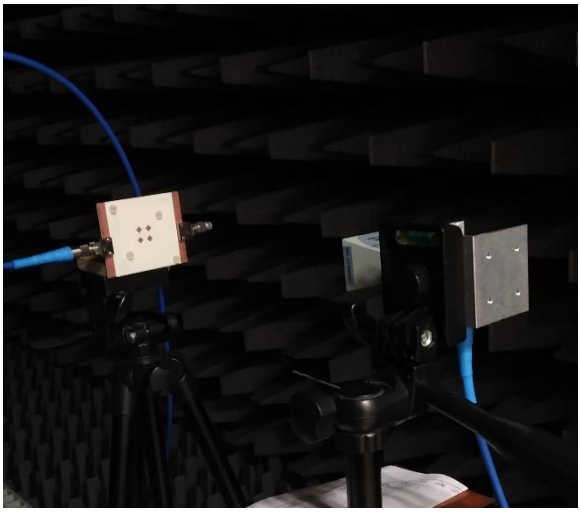

Figure 104: Photograph of the setup in the anechoic chamber, with the transmitting antenna rotated.

The results obtained with this setup are shown below:

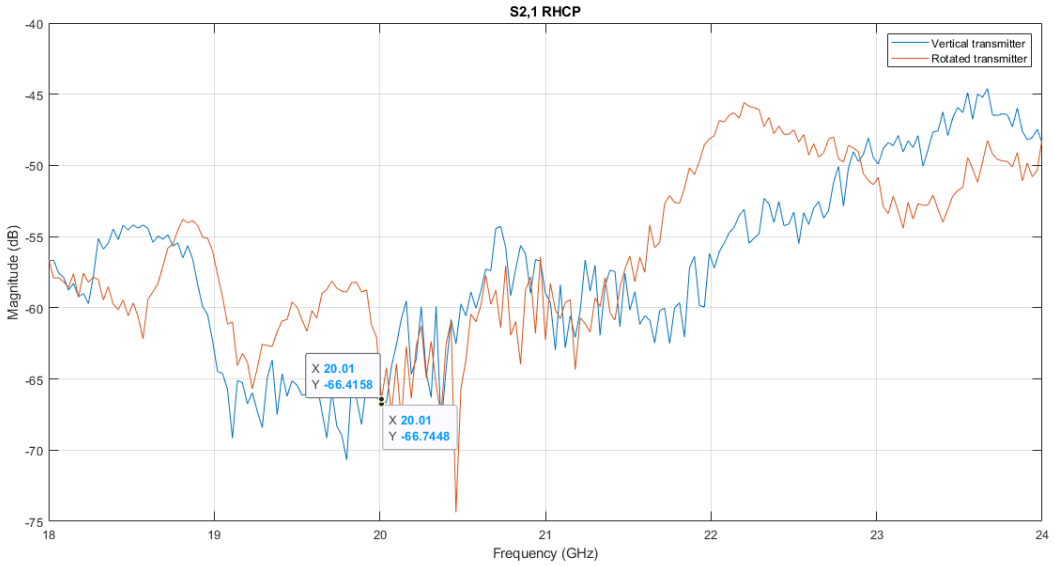

Figure 105: S_{21} of the two positions of the antennas (RHCP).

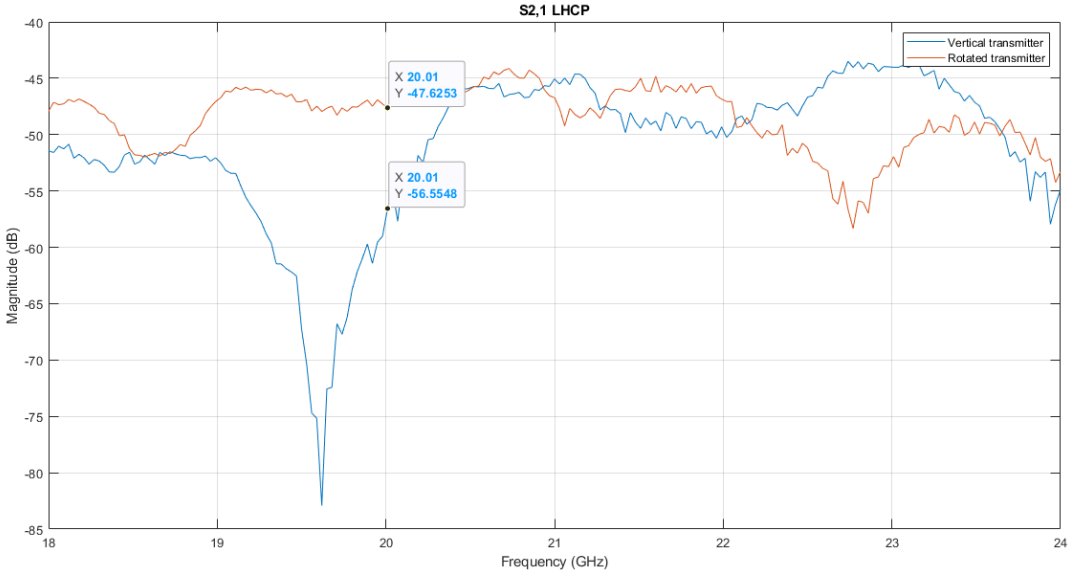

Figure 106: S_{21} of the two positions of the antennas (LHCP).

With the data of Figure 105 and Figure 106, the calculations of the axial ratio can be made in function of the frequency and also presented in graphs in Figure 107 and Figure 108.

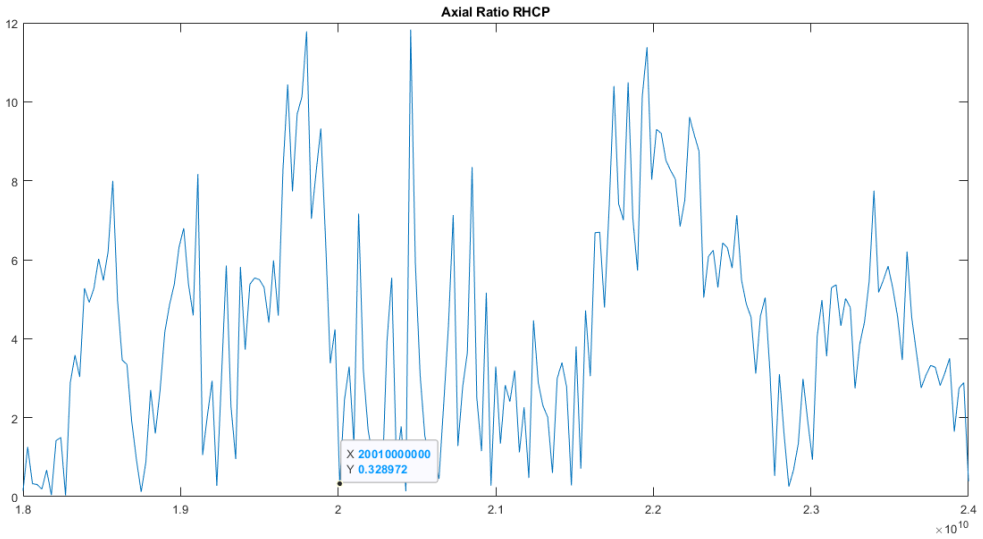

Figure 107: Axial ratio of the RHCP antenna in function of frequency.

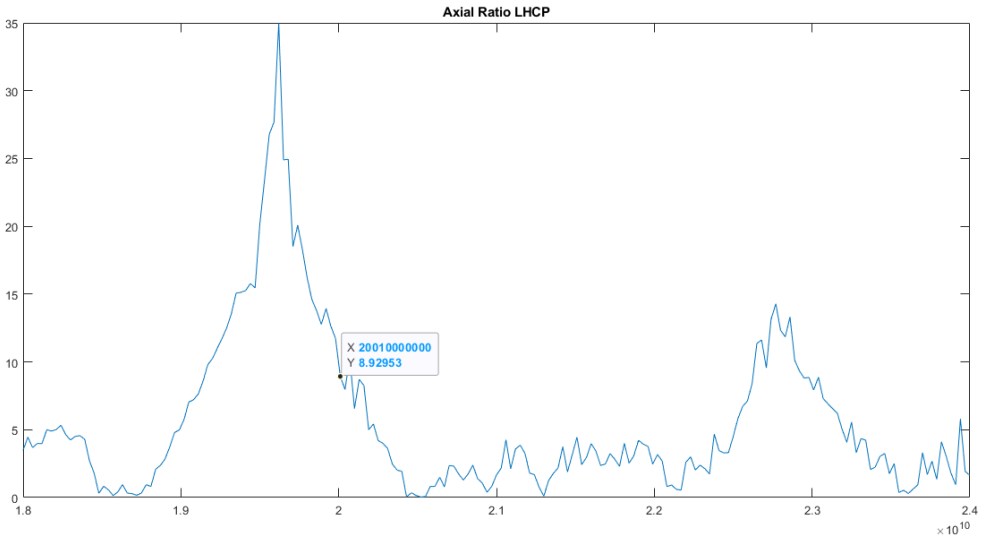

Figure 108: Axial ratio of the LHCP antenna in function of frequency.

Finally, by measuring the S_{21} of a reference receiving antenna (see Figure 109) one can indirectly calculate the gain.

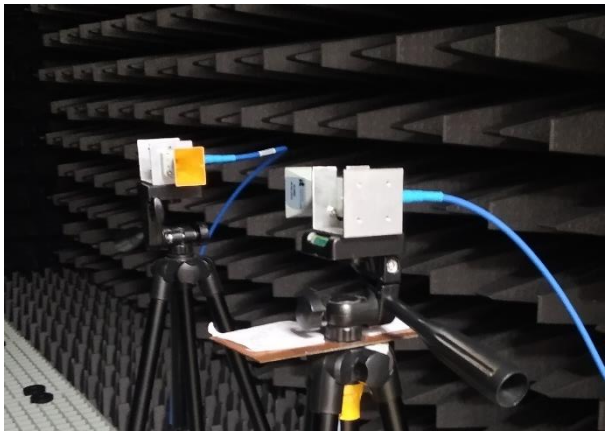

Figure 109: Measurement of the S_{21} of the reference antenna.

The antenna used for this purpose was a broadband horn antenna (LB-180400-KF), which has a gain of approximately 13dB at 20GHz (see Figure 110)

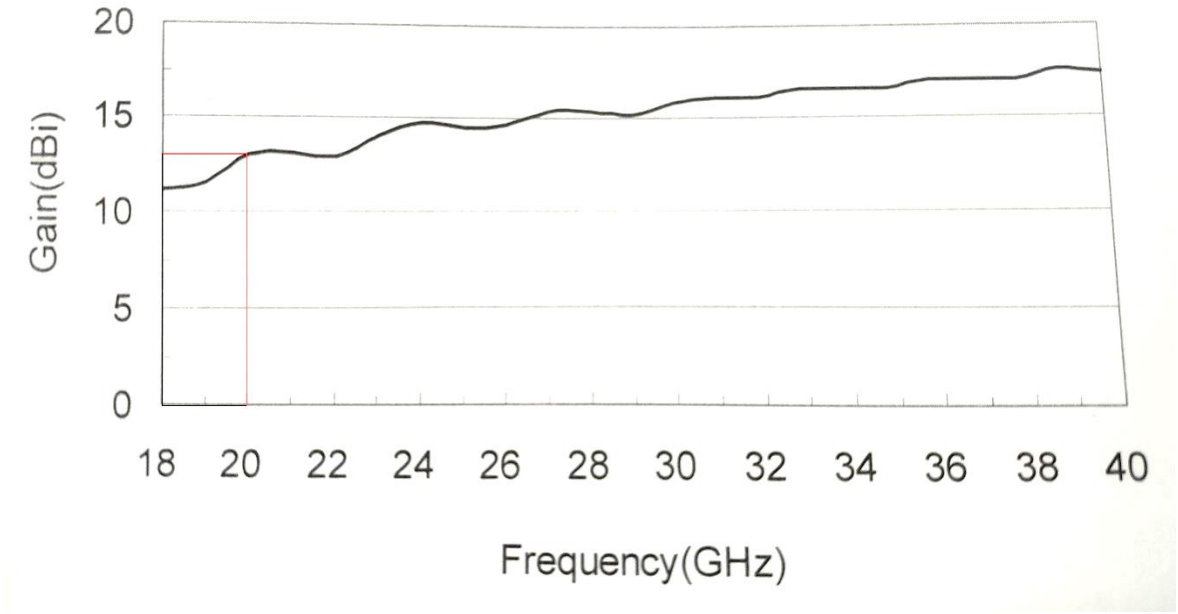

Figure 110: Graph of the reference antenna gain.

Then, by using this known gain and both measurements of the S_{21} of the antennas, the gain of the prototype antenna (AUT - Antenna Under Test) can be calculated, at the operating frequency by the following:

$$G_{AUT} = G_{ref} - \left(S_{2,1_{ref}} - S_{2,1_{AUT}} + PLF\right)[dB]$$

This is known as the substitution method. The gain of the RHCP antenna at the operating frequency is then $G_{RHCP,vertical} = -18dB$ and $G_{RHCP,horizontal} = -18dB$. Thus, the overall gain, by adding the squared contributions (of the vertical and horizontal

gains) and doing the square root of the result, would be $G_{RHCP} = -16dB$. The gain of the LHCP antenna is $G_{LHCP,vertical} = -8dB$ and $G_{LHCP,vertical} = 1dB$, so the overall gain is $G_{LHCP} = 1dB$.

In Table 14 is the summary of the comparison between simulated and measured parameters of the prototype.

	Parameter	Simulation		Measurement	
		@ 20GHz	LB	@ 20GHz	LB
RHCP	S11	-10.6 dB	16.5-21.2 GHz (24%)	-4 dB	20.3-21.1 GHz (4%)
	Gain	7.8 dB	-	-16 dB	-
	Axial Ratio	1.6 dB	19.2-21 GHz (9%)	0.3 dB	≈ 0
LHCP	S11	-16.3 dB	16.8-20.6 GHz (19%)	-20.8 dB	19.5-21.1 GHz (8%)
	Gain	8.8 dB	-	1 dB	-
	Axial Ratio	2.3 dB	19.9-21.1 GHz (6%)	8.9 dB	20.3-21.3 GHz (5%)

Table 14: Summary of simulated vs measured parameters.

5 Conclusions and future work

5.1 Conclusions

When manufacturing the antenna of Figure 99 and Figure 100 it was noted that due to the limited precision of the manufacturing tools and the small distance between the two slots in each single antenna element, the slots seemed to have merged. This could be a problem in the performance of the antenna since the distance between slots impacts the radiation and coupling of the slot.

Shown in Figure 101 is the measured S_{11} of the right polarized (RHCP) antenna compared to the simulated. By analyzing the line corresponding to the measured S_{11}, it can be observed that at the project frequency the antenna has an S_{11} of over −10dB. This means the prototype isn't properly radiating as an antenna at 20GHz. The band in which the S_{11} is smaller than -10dB is in a slightly higher frequency, between 20.3GHz and 21.1GHz. This result isn't satisfactory considering the initial requirements included the antenna being wideband and operating at the center frequency of 20GHz.

While the simulated results still showed promise in relation to this aspect, the measurements of the real prototype show that the design should have been more conservative in terms of margin for errors.

In Figure 102 is the comparison of the measured and simulated S_{11} of the left polarized (LHCP) antenna. In this case the results are better than in the previous. The measured S_{11} has acceptable values (<-10dB) around the center frequency, from 19.5GHz to 21.1GHz. Therefore, a bandwidth of about 1.6GHz is accomplished. While this isn't the ideal outcome, it is still better than the results obtained for the RHCP configuration.

The next step in the procedure was the measurements of the reception of a signal. With the measurement of two orthogonal positions in the configurations of Figure 103 and Figure 104, the axial ratio could then be calculated. This axial ratio (Figure 107 and Figure 108) has a very irregular pattern. In the simulated antenna, an irregular pattern was also obtained in the axial ratio graph, although with less variations than the measured version. This irregular pattern in the simulated axial ratio could be due to spurious feed radiation, interference between lines or inefficient feed design (for example in the usage of quarter-wavelength transformers which are frequency-

dependent). Even though several configurations of the feed line were attempted (using different characteristic impedance for the lines, different quarter-wavelength transformers, less corners in the lines…), none of them showed to improve this aspect. One configuration to try would be the design of the hybrids with a characteristic impedance of 100Ω. It isn't then very surprising that the axial ratio calculated from the measurements doesn't offer better results. Adding to the already described possible sources of error, the manufacturing and measurement errors also contribute to a poor outcome.

In the RHCP antenna configuration, the calculated axial ratio (Figure 97) is 0.3dB (< 3dB so circular polarization is confirmed). However, this circular polarization isn't assured for a band of frequencies since, as can be seen, the axial ratio has a very unpredictable behavior.

For the LHCP antenna configuration, the calculated axial ratio (Figure 108) has a very high value of 8.9dB. This means the antenna isn't circularly polarized at that frequency, which was one of the requirements of the project.

The gain of the antenna was then calculated at the center frequency, with the transmitting and receiving antennas aligned, as described in the previous section (4.2). This method introduces several errors into the measurements and doesn't account for the deviations in the main lobe direction (which have been pointed out to exist in the simulated results in 4.1). The gain values obtained were much lower than expected, since the values simulated are in the order of 7-9 dBi and the ones obtained are below 0dBi.

The purpose of this dissertation was the development of a circularly polarized aperture coupled microstrip antenna, using a quadrature hybrid coupler for the feed. This was accomplished by simulation in CST and the antenna had the desired performance. The incorporation of the hybrid coupler allowed for a wider bandwidth and each input terminal of the hybrid gives a different direction of circular polarization (left or right).

This antenna was then incorporated into a 2x2 array, with half-wavelength spacing and 90º progressively rotated elements. The array should have enhanced gain compared to the individual element and larger circular polarization bandwidth. This array should maintain the characteristics of the previously modelled antenna – wide bandwidth and circular polarization. When simulated without the feedlines, the array had performance

closer to the desired than after the addition of the feedlines, which leads to believe the lines are the issue due to spurious feed radiation and interference between the lines. Perhaps another routing solution, or the avoidance of quarter-wavelength transformers due to their frequency-dependence, would deliver better results. The problem could also be related with the fact that the feeding lines of the array don't have equalized lengths in all elements.

It was also considered pertinent the study of the impact of vias around the patches in the array's mutual coupling. This proved to be unsuccessful since it didn't appear to have a significant impact on the results and was therefore discarded.

Overall, even though not all the requirements were fulfilled, pertinent observations and conclusions could be drawn from this work. The step-by-step building of the final prototype enabled a more detailed viewing of what happened to the performance of the antenna as the structures got more complex and thus which sections of the work could be further explored and optimized.

5.2 Future work

To improve the work done in this dissertation, some suggestions are:

- Look for a configuration of the feeding lines of the array that doesn't degrade the overall performance of the antenna and that aren't so frequency dependent
- Research a technique that reduces the mutual coupling of the array (in alternative to the addition of vias)
- Make a broadband quadrature hybrid coupler
- Transform the structure into a dual-band antenna by stacking two patches and designing a dual-band quadrature hybrid coupler, to allow implementation in different satellites

References

[1] A. A. Huurdeman, *The Worldwide History of Telecommunications*. Hoboken, NJ, USA: John Wiley & Sons, Inc., 2003. doi: 10.1002/0471722243.

[2] D. W. Ball, *Maxwell's Equations of Electrodynamics: An Explanation*. SPIE, 2012. doi: 10.1117/3.1001007.

[3] C. Balanis, *Modern Antenna Handbook*. Wiley, 2008. doi: 10.1002/9780470294154.

[4] R. A. Johnson and H. Jasik, "Antenna engineering handbook /2nd edition/," 1984.

[5] C. A. Balanis, "Antenna Theory: Analysis and Design," 1982.

[6] S. Vajha and S. N. Prasad, "Design and modeling of proximity coupled patch antenna," *2000 IEEE-APS Conference on Antennas and Propagation for Wireless Communications (Cat. No.00EX380)*, pp. 43–46, 2000.

[7] J. T. Obenchain, "A Technical Assessment of Aperture-coupled Antenna Technology," 2014. Accessed: Dec. 22, 2021. [Online]. Available: https://digitalcommons.liberty.edu/honors/418

[8] P. J. Soh, M. K. A. Rahim, A. Asrokin, and M. Z. A. Abdul Aziz, "Design, Modeling, and performance Comparison of feeding techniques for a Microstrip Patch Antenna," *Jurnal Teknologi*, vol. 47, no. 1, Dec. 2007, doi: 10.11113/jt.v47.270.

[9] F. Croq and A. Papiernik, "Stacked slot-coupled printed antenna," *IEEE Microwave and Guided Wave Letters*, vol. 1, pp. 288–290, 1991.

[10] H. N. Awl *et al.*, "Bandwidth Improvement in Bow-Tie Microstrip Antennas: The Effect of Substrate Type and Design Dimensions," *Applied Sciences*, vol. 10, p. 504, 2020.

[11] R. C. Hall and J. R. Sanford, “Performance enhancements for aperture coupled microstrip antennas,” *IEEE Antennas and Propagation Society International Symposium 1992 Digest*, pp. 1040–1043 vol.2, 1992.

[12] M. Grilo and F. Correra, “Rectangular patch antenna on textile substrate fed by proximity coupling,” *Journal of Microwaves, Optoelectronics and Electromagnetic Applications*, vol. 14, pp. SI103–SI112, Dec. 2015.

[13] K. Moradi and S. Nikmehr, “A dual-band dual-polarized microstrip array antenna for base stations,” *Progress in Electromagnetics Research-pier*, vol. 123, pp. 527–541, 2012.

[14] Y. Su, Y. Liu, Y. Zhou, J. Yuan, H. Cao, and J. Shi, “Broadband LEO Satellite Communications: Architectures and Key Technologies,” *IEEE Wireless Communications*, vol. 26, pp. 55–61, 2019.

[15] B. Di, L. Song, Y. Li, and H. V. Poor, “Ultra-Dense LEO: Integration of Satellite Access Networks into 5G and Beyond,” *IEEE Wireless Communications*, vol. 26, no. 2, pp. 62–69, Apr. 2019, doi: 10.1109/MWC.2019.1800301.

[16] L. J. Ippolito, *Satellite communications systems engineering : atmospheric effects, satellite link design, and system performance*. John Wiley & Sons, 2008.

[17] Newell *et al.*, “IEEE Standard Definitions of Terms for Antennas,” 1993. doi: 10.1109/IEEESTD.2014.6758443.

[18] J. L. Volakis, *Antenna Engineering Handbook*. McGraw-Hill Education, 2007.

[19] B. D., E. Sulic, W. S. T. Rowe, K. Ghorbani, and S. Joh, “Advancements in Automotive Antennas,” in *New Trends and Developments in Automotive System Engineering*, InTech, 2011. doi: 10.5772/13368.

[20] “Classification of Polarization.” http://hyperphysics.phy-astr.gsu.edu/hbase/phyopt/polclas.html (accessed Oct. 28, 2021).

[21] K.-L. Wong, *Compact and Broadband Microstrip Antennas*. New York, USA: John Wiley & Sons, Inc., 2002. doi: 10.1002/0471221112.

[22] D. M. Pozar, “A Review of Aperture Coupled Microstrip Antennas: History, Operation, Development, and Applications,” *University of Massachusetts at Amherst*, pp. 1–9, 1996.

[23] James J. and Hall P., Eds., *Handbook of microstrip antennas*, vol. 28. The Institution of Engineering and Technology, 1989.

[24] R. B. Waterhouse, *Microstrip Patch Antennas: A Designer’s Guide*. Boston, MA: Springer US, 2003. doi: 10.1007/978-1-4757-3791-2.

[25] K. Işeri, “Analysis of Dual-Polarized Aperture-Coupled Microstrip Antennas with H-shaped Slots and Equivalent Circuit Modeling of H-shaped Slots,” M.S. Thesis, Middle East Technical Univ., 2012. [Online]. Available: https://avesis.metu.edu.tr/yonetilen-tez/a273647c-66c4-4947-97cd-aa59bd9ff5f7/analysis-of-dual-polarized-aperture-coupled-microstrip-antennas-with-h-shaped-slots-and-equivalent-circuit-modeling-of-h-shaped-slots

[26] H. Liu, A. Qing, and Z. Xu, “Design of Switchable Circularly-Polarized Phased Array Based on Sequential Rotation and 45-degree Rotated Linearly Polarized Elements,” *2020 IEEE International Symposium on Antennas and Propagation and North American Radio Science Meeting*, pp. 563–564, 2020.

[27] R. A. Sainati, *CAD of Microstrip Antennas for Wireless Applications*. USA: Artech House, Inc., 1996.

[28] Z. Aijaz and S. Shrivastava, “Effect of the Different Shapes Aperture Coupled Microstrip Slot Antenna,” *Int J Electron Eng*, vol. 2, Dec. 2010.

[29] Y. Cailloce, M. Himdi, D. Thouroude, and J. P. Daniel, “Analysis of aperture-coupled microstrip antenna using the segmentation method,” *Electronics Letters*, vol. 32, pp. 1047–1048, 1996.

[30] X. H. Yang and L. Shafai, “Characteristics of aperture coupled microstrip antennas with various radiating patches and coupling apertures,” *IEEE Transactions on Antennas and Propagation*, vol. 43, pp. 72–78, 1995.

[31] V. Rathi, G. Kumar, and K. Ray, “Improved coupling for aperture coupled microstrip antennas,” *IEEE Transactions on Antennas and Propagation*, vol. 44, pp. 1196–1198, 1996.

[32] S. Sherlock, “Circularly Polarized Microstrip Antenna Array,” 2016. [Online]. Available: https://loop.dcu.ie/mod/url/view.php?id=448779.

[33] S. S. Gao, L.-W. J. Li, M.-S. Leong, and T. S. Yeo, “A broad-band dual-polarized microstrip patch antenna with aperture coupling,” *IEEE Transactions on Antennas and Propagation*, vol. 51, pp. 898–900, 2003.

[34] S. Foo, “A dual polarized CPW-Fed aperture-coupled stacked patch,” *2009 13th International Symposium on Antenna Technology and Applied Electromagnetics and the Canadian Radio Science Meeting*, pp. 1–4, 2009.

[35] S. Drabowitch, A. Papiernik, H. D. Griffiths, J. Encinas, and B. L. Smith, *Modern Antennas*. Boston, MA: Springer US, 2005. doi: 10.1007/978-0-387-26231-4.

[36] S. Silver, *Microwave Antenna Theory and Design*. The Institution of Engineering and Technology, Michael Faraday House, Six Hills Way, Stevenage SG1 2AY, UK: IET, 1984. doi: 10.1049/PBEW019E.

[37] R. Oostlander, Y. M. M. Antar, A. Ittipiboon, and M. Cuhaci, “Aperture coupled microstrip antenna element design,” *Electronics Letters*, vol. 26, pp. 224–225, 1990.

[38] P. L. Sullivan and D. H. Schaubert, “Analysis of an aperture coupled microstrip antenna,” *IEEE Transactions on Antennas and Propagation*, vol. 34, pp. 977–984, 1986.

[39] M. Bai, J. Xing, Z. Wang, and B. Yan, “Design of an H-shape cross slotted aperture-coupled microstrip patch antenna,” *2012 IEEE International Workshop on Electromagnetics: Applications and Student Innovation Competition*, pp. 1–3, 2012.

[40] J.-S. Jeon, “Design of wideband dual-polarized microstrip antennas,” *2011 XXXth URSI General Assembly and Scientific Symposium*, pp. 1–4, 2011.

[41] J. N. Sahalos, *Orthogonal Methods for Array Synthesis*. Chichester, UK: John Wiley & Sons, Ltd, 2006. doi: 10.1002/0470028548.

[42] J.-Y. Sze and K.-L. Wong, “Bandwidth enhancement of a microstrip-line-fed printed wide-slot antenna,” *IEEE Transactions on Antennas and Propagation*, vol. 49, pp. 1020–1024, 2001.

[43] B. Hammu-Mohamed, Á. Palomares-Caballero, C. Segura-Gómez, F. G. Ruiz, and P. Padilla, “SIW Cavity-Backed Antenna Array Based on Double Slots for mmWave Communications,” *Applied Sciences*, vol. 11, p. 4824, 2021.

[44] F. Croq and D. M. Pozar, “Millimeter-wave design of wide-band aperture-coupled stacked microstrip antennas,” *IEEE Transactions on Antennas and Propagation*, vol. 39, pp. 1770–1776, 1991.

[45] C.-H. Jung, S.-H. Lim, and N.-H. Myung, “Analysis of an H-shape cross slotted aperture-coupled microstrip patch antenna,” in *2009 Asia Pacific Microwave Conference*, Dec. 2009, pp. 1890–1893. doi: 10.1109/APMC.2009.5384207.

[46] Biao Li, Ying-Zeng Yin, Wei Hu, Yang Ding, and Yang Zhao, “Wideband Dual-Polarized Patch Antenna With Low Cross Polarization and High Isolation,” *IEEE Antennas and Wireless Propagation Letters*, vol. 11, pp. 427–430, 2012, doi: 10.1109/LAWP.2012.2195149.

[47] A. Vaziri, M. Kaboli, and S. A. Mirtaheri, “Dual-polarized aperture-coupled wideband microstrip patch antenna with high isolation for C-Band,” in *2013 21st Iranian Conference on Electrical Engineering (ICEE)*, May 2013, pp. 1–4. doi: 10.1109/IranianCEE.2013.6599842.

[48] A. Pandey, *Practical Microstrip and Printed Antenna Design*. Artech House, 2019.